THE DECAY OF ^{185}Os

THE DECAY OF ^{185}Os

by

WILLIAM BRIAN COOK, B.Sc. (Eng.)

A Thesis

Submitted to the Faculty of Graduate Studies

in Partial Fulfilment of the Requirements

for the Degree

Master of Science

McMaster University

September 1968

MASTER OF SCIENCE (1968) McMASTER UNIVERSITY
(Physics) Hamilton, Ontario.

TITLE: The Decay of ^{185}Os

AUTHOR: William Brian Cook, B.Sc.,(Eng.) Queens University

SUPERVISOR: Professor M. W. Johns

NUMBER OF PAGES: vii, 93

SCOPE AND CONTENTS:

The decay of 94 day ^{185}Os to levels in ^{185}Re has been studied, using Ge(Li), NaI(Tl), and Si(Li) detectors. The internal conversion spectrum was investigated using the Chalk River $\pi\sqrt{2}$ β-spectrometer. The decay scheme is discussed and some spin assignments are suggested.

ACKNOWLEDGEMENTS

I wish to express my appreciation to Professor M. W. Johns for his support and guidance. Also I wish to thank Dr. L. Schellenberg and Dr. Z. Sujkowski for their helpful discussions. For making available the $\pi\sqrt{2}$ spectrometer I am indebted to Dr. R. Graham and Dr. J. Geiger and to Mrs. J. Merritt for helping with the chemistry.

Assistance from other members of the Beta and Gamma Spectroscopy Group is gratefully acknowledged. Thanks are also due to Mrs. Helen Kennelly for her typing.

TABLE OF CONTENTS

LIST OF FIGURES

LIST OF TABLES

CHAPTER I

INTRODUCTION

In nuclear spectroscopy one is interested in learning as much as possible about the properties of the various energy levels in nuclei and in experimentally verifying models and theories derived to explain nuclear properties. Spin, parity and energy of the state are some of the nuclear properties of interest. Although most excited states are too short-lived to determine these properties while the nucleus is in that particular state, they can be deduced from a study of transitions between the level in question and other levels for which the spin, parity and energy are known.

The purpose of this chapter is to discuss the theoretical aspects of nuclear spectroscopy needed to interpret the experimental measurements to be discussed later. Also, a section on nuclear models relevant to this thesis is included.

1.1 Beta Decay

There are four types of physical forces known: nuclear forces (arising from the π-meson field), electromagnetic forces, weak interactions and gravitational forces, in order of decreasing strength. Representative numbers describing comparative orders of magnitude for these interactions are 10, 10^{-2}, 10^{-23} and 10^{-45},

respectively (Preston 1962).

The weak interaction manifests itself in nuclei in β-decay which is a nuclear transformation accompanied by the emission of an electron or positron, or by the capture of an orbital electron. The three modes of decay are listed below:

(i) The reaction $n \rightarrow p + e^- + \bar{\nu}$ describes the decay of neutron-rich nuclei and the free neutron, a neutron decaying into a proton, electron and antineutrino.

(ii) The reaction $p \rightarrow n + e^+ + \nu$ describes the decay of proton-rich nuclei, a proton decaying into a neutron, positron and neutrino. It cannot take place with free protons because of energy considerations (the proton mass being less than the products).

(iii) The reaction $p + e^- \rightarrow n + \nu$ describes the capture of an orbital electron by a proton with a resulting transformation into a neutron and neutrino. This process is explained in more detail in Chapter II.

In the first two cases shown above, the excess energy of the reaction is shared statistically between the electron and the neutrino; hence, the energy distribution for each particle is a continuum from zero up to the maximum beta energy available. This distribution appeared to violate the conservation of energy; furthermore, since the number of nucleons does not change, the spin (defined as the vector sum of the intrinsic

angular momentum and orbital angular momentum of all the nucleons in the nucleus) of the nucleus remains integral for even-A or half integral for odd-A during a β-decay, and since the electrons' angular momentum is half-integral, the law of conservation of angular momentum also appeared to break down. Pauli (1934) suggested that the β-decay processes were accompanied by the emission of a new particle with spin $\hbar/2$, no charge or mass, and a very low cross-section for interaction with matter. This particle, called the neutrino, was finally detected by Reines and Cowan (1960) who used the inverse reaction $p+\bar{\nu}\rightarrow n+e^+$.

Fermi (1934) incorporated Pauli's hypothesis into the first successful theory of β-decay; the theory was constructed in analogy with that for electromagnetic interactions. From perturbation theory, the probability for the interaction may be written as

$$W(E) = \frac{2\pi}{\hbar} |\langle\psi_f^* \phi_f^* | H_\beta | \psi_i \phi_i \rangle|^2 \rho_e$$

where ψ_i and ψ_f represent initial and final nuclear states, ϕ_i and ϕ_f initial and final lepton states. H_β is the interaction Hamiltonian and ρ_e is the density of final states. In addition to the operators which convert neutrons into protons, neutrinos into electrons, etc., there may be still other operators present. When the conditions of relativistic invariance and of conservation of momentum and of angular momentum are imposed, five possible combinations exist: the

scalar, pseudoscalar, vector, axial vector and tensor interactions; they are denoted by S,P,V,A,T respectively. Of these, experiments (Segrè 1964) have shown that only the vector and axial vector combinations occur in nature. The V-interaction is the one used first by Fermi and results in the Fermi selection rules; the A-interaction yields the Gamow-Teller selection rules. A brief listing of the most common selection rules for spin and parity (π) is shown below.

Type of Transition	Fermi (Vector)		Gamow-Teller (Axial Vector)	
Allowed	$\Delta I=0$	$\Delta\pi$=No	$\Delta I=0,\pm 1$	$\Delta\pi$ =No
First Forbidden	$\Delta I=0,\pm 1$	$\Delta\pi$=Yes	$\Delta I=0,\pm 1,\pm 2$	$\Delta\pi$ =Yes
Second Forbidden	$\Delta I=\pm 2$	$\Delta\pi$=No	$\Delta I=\pm 2,\pm 3$	$\Delta\pi$ =No

Upon integrating the transition probability W over appropriate variables, the β-decay process may be written as

$$N(p)dp = C|M|^2 F(Z,E) p^2 (E_o - E)^2 Sn\, dp$$

Here $N(p)dp$ is the probability that the β-particles are emitted between p and p+dp where p is their momentum. C is a constant, M is the nuclear matrix element, F(Z,E) is the Fermi function which corrects for the Coulomb interaction between the nucleus and the emerging electrons (assumed plane waves). E_o is the maximum energy of the electrons, E is the energy of the electrons and Sn is the shape factor which corrects the expression when higher degrees of forbiddenness is required (n indicates the degree of forbiddenness).

Integrating N(p)dp over all possible momenta yields the total probability of decay

$$\lambda = \frac{\ell n 2}{T_{1/2}} = C|M|^2 f(Z,E)$$

where $T_{1/2}$ is the half-life for the decay and f(Z,E) is a tabulated function of Z and E; hence, the product $fT_{1/2}$ can be found.

The quantity $fT_{1/2}$ is called the comparative half-life; it is inversely proportional to the square of the nuclear matrix element. In practice, one can only work out $f_oT_{1/2}$ since Sn is not uniquely defined for most forbidden decays. The values of $f_oT_{1/2}$ vary over a wide range and thus can give a rough indication of the degree of forbiddenness of a transition.

Type		ΔI	Δπ	log f_o $T_{1/2}$
allowed	super allowed	0	no	3.5 ± 0.5
	allowed unhindered	0,1	no	5 ± 1
	allowed hindered	0,1	no	6 ± 1
first forbidden (non unique)		0,1	yes	6.5 ± 3
first forbidden (unique)		2	yes	9.6 ± 2
second forbidden		2,3	no	13
third forbidden		3,4	yes	18

1.2 The Electromagnetic Interaction

(a) Gamma Ray Emission

After β-decay the nucleus can be left in an excited state which is de-excited to the ground state by a direct interaction or by a series of cascade events involving some intermediate states. The transitions between the nuclear states are accomplished predominantly by the emission of electromagnetic radiation.

This radiation is classified as being of multipole order λ when the quantum carries away λ units of angular momentum. This angular momentum is related to the spin change between the nuclear states between which the transition took place. There is a further classification into electric (E) or magnetic (M) transitions depending on whether a parity change is involved. For electric transitions $\Delta\pi=(-1)^{\lambda}$, while for magnetic transitions $\Delta\pi=(-1)^{\lambda+1}$ ($\Delta\pi=1$ means no parity charge, $\Delta\pi = -1$ means a parity change). The selection rule on the possible initial and final values of the nuclear spin, I_i and I_f for a given λ is given by the triangle relation $|I_i-I_f|\leqslant\lambda\leqslant I_i+I_f$. Transitions for which $I_i=I_f=0$ are forbidden and no transitions occur with $\lambda=0$.

The transition probability for emission of a photon of energy $\hbar\omega$ with the nucleus going from state i to state f is (Preston 1962)

$$T(\sigma,\lambda) = \frac{8\pi(\lambda+1)}{\lambda[2\lambda+1)!!]^2} \frac{k^{2\lambda+1}}{\hbar} B(\sigma,\lambda)$$

where $k = \omega/c$ and the reduced matrix element is

$$B(\sigma\lambda, J_i \to J_f) = (2J_i+1)^{-1} \sum_{M_i,M_f} |\langle f|O_{\lambda M}|i\rangle|^2$$

where $O_{\lambda M}$ stands for $E_{\lambda M}$ or $M_{\lambda M}$ the electric and magnetic operators repsectively, σ refers to the type of transition, electric or magnetic. The quantity $B(\sigma,\lambda)$ may be evaluated by use of nuclear wavefunctions obtained from a model. The simplest model to assume is that the transition is due to the vibration of a single nuclear proton. The transition probabilities derived on this assumption are called the single-particle or Weisskopf (1951) estimates. Actual transition rates are conveniently expressed in terms of these "Weisskopf units".

It is seen that the transition probability decreases rapidly as λ increases. Thus for either electric or magnetic transitions, only the lowest multipole order allowed by angular momentum and parity considerations will be present with appreciable intensity. However, there can be competition between electric and magnetic transitions since the ratio of E and M transition probabilities for the same multipole order is $\sim(\frac{M_c R}{\hbar})^2$ where R is the nuclear radius. Such competition is found most often between M1 and E2 transitions because collective effects in deformed nuclei enhance the E2 transition probability to such an extent that it can be comparable with

that for M1 transitions.

(b) Internal Conversion

A mode of decay which always competes with gamma emission is internal conversion. In this process, the excitation energy of the nucleus is transferred by the electromagnetic fields to one of the atomic electrons which is ejected from the atom with an energy $E_\gamma - B_j$ (B_j is the atomic binding energy of the j^{th} shell). For any given gamma transition, several competing conversion lines will appear, corresponding to internal conversion of electrons from the K, L_1, L_2, L_3 etc. shells. Since the electrons closest to the nucleus have the greatest probability of interacting with it, the K lines are stronger than the L lines, the L lines are stronger than the M lines and so on.

The internal conversion coefficient is defined as the ratio $\alpha = \frac{T_e}{T_\gamma}$ (where T_e and T_γ are the probabilities of internal conversion and of photon emission respectively) which, of course, equals the observable quantity N_e/N_γ, that is, the ratio of the total number of internal conversion electrons (from a given shell) and the total number of gamma rays emitted in the same nuclear transition. The theoretical calculation of this expression is in principle straightforward; the relevant theory is the relativistic Dirac theory of the electron. The first complete set of calculated internal conversion coefficients was published by Rose and co-workers (1951). These

calculations were based on what is generally referred to as the point nucleus approximation. In this approximation the nucleus is regarded as a point source of a virtual electromagnetic field. Consequently no detail of nuclear structure enters the theory. The internal conversion coefficients then simply depend on the transition energy k, the atomic number Z, the atomic shell or subshell from which the electron is emitted A, the multipolarity or angular momentum of the electromagnetic field L, and finally on the parity of the field. Thus,

$$\alpha = \frac{N_e}{N_\gamma} = \alpha(k,Z,A,L,\Delta\pi)$$

By 1954 experimentally measured internal conversion coefficients were reported to be in disagreement with the theoretical values obtained in the point nucleus approximation (Wapstra and Nijgh (1956), Feather (1955), and Sunyar (1955)). These discrepancies had been theoretically predicted by Sliv (1951), who pointed out that the finite size of the nucleus under certain circumstances is expected to give rise to large deviations from the values obtained in the point nucleus approximation. The effects due to the finite size of the nucleus are expected to be particularly large for K-conversion electrons, which are s-electrons and which have a maximum probability of being in the immediate vicinity of the nucleus and in fact, they penetrate into the nucleus itself. The effects are expected to increase with Z, partly due to the

increased nuclear volume for heavier elements and partly due to the increased Coulomb attraction from the heavier charged high Z nuclei. Finally, the finite size effects are expected to be particularly pronounced for the M1 conversion process (the conversion implying s-1/2 initial state$\rightarrow s^{1}/_{2}$ or $d^{3}/_{2}$ final state, $s^{1}/_{2} \rightarrow s^{1}/_{2}$ being the dominant branch). Therefore in the case of M1 transitions, there are s-electron wavefunctions in both the initial and final states, providing maximum overlap between the electron and nuclear wavefunctions (Gerholm and Pettersson 1963).

Due to these difficulties new theoretical calculations, in what is known as the finite size approximation, were performed by Rose (1958) and Sliv and Band (1956, 1958). The effect of the finite size of the nucleus is to give rise to a static deformation of the electron wavefunctions. This effect causes a change in the radial matrix elements and consequently also in the internal conversion coefficients.

However, as pointed out by Church and Weneser (1956), there are exceptional cases where large deviations from the results obtained in the static finite size approximation are to be expected. They realized that the interaction to a great extent takes place in the immediate vicinity of the nucleus and, in fact, within the nucleus itself. The interaction in the interior of the nucleus is not of the same form as in the extra nuclear region. The conversion matrix element should be

composed of one part to represent the extra nuclear process ("normal" static finite size corrected conversion matrix element) and another part to represent the fraction of the conversion process taking place in the nuclear interior. Since these "penetration matrix elements" depend on the detailed nuclear structure, the internal conversion coefficients are not entirely independent of the details of a specific nuclear model. This is the difference between the tables of Rose and Sliv and Band; Sliv and Band's tables hold for the "surface current model" and consequently, do take into account a contribution caused by penetration effects (relevant to this model). Rose's calculations are model independent since he restricted his calculations to the extra nuclear region.

The internal conversion coefficients (α_K,α_L, etc. and their ratios (α_K/α_L, $\alpha_{L_1}/\alpha_{L_2}/\alpha_{L_3}$) are very useful in determining the type of transitions between nuclear levels. It should be noted that all the conversion coefficients do not have to be determined by an absolute measurement. If the conversion coefficient of one line is known, one can determine the conversion coefficients of the other lines by a relative method. The relevant equation is

$$\alpha_j = \alpha_s \frac{N_{es}}{N_{\gamma s}}$$

where α_j is the conversion coefficient to be found, α_s is the known conversion coefficient, and N_{es} and $N_{\gamma s}$ are the number of electrons and gamma rays relative to the known line.

1.3 The Shell Model

By 1949, a large amount of experimental evidence had been accumulated which suggested shell structure or quasi single-particle behaviour for the nucleus. The discontinuities in nuclear properties associated with the magic numbers (2, 8, 14,20, 28, 50, 82, 126) were recognized. The shell model was independently proposed by Mayer (1949,1950) and Haxel, Jensen and Suess (1949,1950). The model assumes that each nucleon moves in a static central potential created by the averaged interaction between the other nucleons. In a single particle model, the existence of a large gap in the spacing of the energy levels leads to "closed-shell effects" when all the levels are filled up to this energy region. The feature of the shell model which produces such energy gaps at the correct magic numbers is the assumption of a strong spin-orbit coupling of the form $V(\vec{r})\vec{\ell}\cdot\vec{s}$, where $V(\vec{r})$ describes the radial dependence and $\vec{\ell}$ and $\vec{s}$ are the orbital and spin angular momenta. This spin-orbit force leads to a splitting of the degenerate levels into two corresponding to the two possible values of $\vec{j}$ able to be formed from each $\vec{\ell}$-value, namely, $j = \ell \pm 1/2$. The level with the larger j is more tightly bound. Since the magnitude of the splitting increases with the value of $\vec{\ell}$, the effect of the interaction is to depress the higher angular momentum states down to the next shell thereby creating a closed (and now magic) shell.

In the simplest form of the shell model, the extreme single-particle model, the nucleons in the ground state are supposed to have dynamically paired motions so that many of the nuclear properties are due only to the last unpaired nucleon. It is also assumed that the neutron and proton states fill independently. In this model, all the different states which can be formed by k particles with the same (n,ℓ,j) have the same energy.

A more realistic approach considers only the nucleons in closed shells to form an inert core and takes into account the internucleon forces between particles in unfilled orbitals. The interaction in this extended single-particle model is strong enough to remove the above degeneracies but not so strong, compared with the spin-orbit force, that j ceases to be a good quantum number for each nucleon.

Experimentally however, it is found that nuclei with partially filled shells possess large quadrupole moments, level structures characteristic of a rigid rotor, and electric quadrupole transition rates much faster than any simple particle model can explain. In order to resolve these experimental facts, it is essential to use a model which takes into account collective nuclear motion; that is, a model which recognizes the fact that a large number of particles may be involved in cooperative modes of motion of an aspherical character.

1.4 Collective Motions

In the collective theory developed by Bohr and Mottelson (1953), the nucleus was treated macroscopically as a deformable liquid drop interacting with the extra nucleons of the unfilled shell. The deformations are volume preserving ones since nuclear matter is considered essentially incompressible.

To consider vibrations (oscillations about a spherical equilibrium shape), the nucleus is expanded in spherical harmonics

$$R(\theta,\phi) = R_o[1 + \sum_{\lambda=o}^{\infty} \sum_{\mu=-\lambda}^{\lambda} \alpha_{\lambda\mu} Y_\lambda^\mu (\theta,\phi)]$$

where R_o is the radius of the undistorted nuclear surface and the $\alpha_{\lambda\mu}$ are the deformation parameters. Collective motions are described by allowing time variations of the $\alpha_{\lambda\mu}$. It is possible to set up expressions for the kinetic and potential energies and obtain relationships for the frequency of vibration of the surface, ω_λ. These vibrations are called phonons, of order λ, and have associated with them an angular momentum λ, parity $(-1)^\lambda$ and an energy $\hbar\omega_\lambda$. The level structures predicted by the above model agree particularly well with that found experimentally for even-even nuclei and for nuclei with only a few nucleons outside a closed shell.

It is often convenient to change the notation and describe the vibrational behaviour in terms of two other parameters, β (a measure of the total deformation of the nucleus) and γ (a measure of the nuclear asymmetry), which are related

to the $\alpha_{\lambda\mu}$'s. Beta vibrations are oscillations which alter the eccentricity of the nucleus but still preserve its symmetry; gamma vibrations cause the nucleus to lose its axial symmetry.

When there are a large number of particles outside a closed shell (that is, the nucleus has a large permanent deformation), the nucleus can undergo changes in its orientation (rotations) as well as oscillations in its shape (vibrations). By considering the nucleus to be a rigid rotor, the rotational level structure, which is predominant in these nuclei, can be derived. This assumes that the rotational and vibrational motions can be considered separately in the nuclear Hamiltonian. The energy associated with the rotational motion of a state involving an intrinsic energy ε_K is given by

$$E = \varepsilon_K + \frac{\hbar^2}{2\mathcal{J}}[I(I+1)-K^2] - BI^2(I+1)^2$$

The last term results from a weak coupling between rotational and vibrational modes of oscillation. It should be noted here that rotational bands can be built up on collective vibrational states as well as on particle states.

Since odd nuclei have non-zero intrinsic spin, it is necessary to consider the coupling of the particle motions with the collective motions. Therefore, terms involving the component of the particles angular momentum ($\vec{j}$) along the symmetry axis (Ω) and involving rotational particle coupling (analogous to the Coriolis force in classical mechanics) must

be added to the energy expression given above. The latter term is negligible except in two special cases. If a nucleus has two closely spaced particle states differing by one unit in K, important perturbations can result. The other case where the RPC term is important is in a rotational band for which $\Omega = 1/2$.

Due to the fact that nuclei with unfilled shells were found to have a distorted nature, it was realized that a non-spherical potential should have been used in shell model calculations for these nuclei. Nilsson (1955) extended the shell model by calculating the energies of the single particle levels in an anisotropic harmonic oscillator potential. To the oscillator potential with the usual $\vec{\ell}\cdot\vec{s}$ term included, Nilsson added a term proportional to $\vec{\ell}^2$. The strengths of these terms were adjusted so that at zero deformation the energy level scheme predicted was equivalent to that given by a spherical shell model potential. Nilsson's results are presented in the form of graphs which show the energies of the various particle states as a function of deformation and tables which give the wave functions of the states.

In Nilsson's notation, the wave functions are given by

$$\psi_{\alpha\Omega} = \Sigma a_{\ell\Lambda} |N\ell\Lambda\Sigma>$$

where N is the total number of oscillator quanta, ℓ is the orbital angular momentum of the particle and Λ is its component along the symmetry axis. Σ is the component of spin along the symmetry axis; $\Omega = \Lambda + \Sigma$.

CHAPTER II

ORBITAL ELECTRON CAPTURE

Introduction

The process of nuclear decay through capture of an orbital electron and emission of a neutrino resembles β^+-decay in many respects. The initial and final states of the nucleus are identical in the two processes and, because of this, the nuclear matrix element and selection rules for electron capture and positron decay are the same.

The difference between electron capture and β^+-decay arises from the fact that the bound state of an electron in an atomic shell is different from the state of a β-electron falling into a continuous energy spectrum. Also, the neutrino emitted during electron capture has a certain discrete energy. Therefore, there are some differences in the probability of occurrence of the two processes.

2.1 Energetics of the Decay Process

In order to consider the energetics of the electron capture decay process (Rao and Crasemann 1966), it is necessary to define a number of quantities:

W_o = difference in initial and final nuclear masses.

E(G) = energy of atomic electrons in the ground state of the initial atom .

E(G') = energy of atomic electrons in the ground state of the final atom.

E(A') = energy of the atomic electrons in the excited state corresponding to the K, L, or M shell vacancy created by nuclear electron capture.

Q = mass difference between the initial and final atoms in their atomic ground states.

The neutrino energy is then given by

$$q = W_o + E(G) - E(A') \ .$$

But

$$Q = W_o + E(G) - E(G') \ .$$

Therefore

$$q = Q - [E(A') - E(G')] \ .$$

If capture occurs from the X-shell, the excitation energy of the daughter atom is given by

$$E(A') - E(G') = |B(X')| + \Delta E(A')$$

where $|B(X')|$ is the positive binding energy of an electron in the X-shell of the daughter atom and $\Delta E(A')$ is the small residual excitation energy caused by the fact that a reorganization of all the atomic levels is taking place. Usually, $\Delta E(A')$ is neglected, although sometimes without justification. Thus, to a high degree of approximation

$$Q = q + |B(X')| \ .$$

The total decay probability of a nucleus through electron capture is usually expressed as the sum of the probability

of capture of the i different subshells of the atom. In this nonrelativistic approximation, only the K, L_1, M_1, N_1, etc. shells would contribute appreciably to electron capture, since only s(ℓ=0) particles have finite wavefunctions at the origin (Brysk and Rose 1958). However, the small component of the relativistic wavefunction behaves like an ℓ=0 function, although the main component behaves like a p(ℓ=1) wavefunction. Consequently, the L_2, M_2, N_2, etc. shells do contribute to some degree. The L_3 electrons contribute only because the nucleus is of finite extent; the L_3 contribution is of the order of R^2 of the L_2 contribution (where R, the nuclear radius in relativistic units, is given by $0.426\ \alpha\ A^{1/3}$, α being the fine structure constant and A the mass number. (Preston 1962)).

2.2 Probability of K,L,M Capture For Allowed Transitions

There is no allowed capture from the L_3 subshell. The capture probability of the i^{th} electron can be represented in the form (Zyryanova 1963)

$$W_i = \frac{g^2}{2\pi^3} f_i(Q,Z)|M|^2$$

where M is the nuclear matrix element, g is Fermi's β-interaction constant. The functions f_i are defined as follows:

$$f_K = \frac{\pi}{2} G_K^2 (Q-B_K)^2 \qquad f_{L_1} = \frac{\pi}{2} G_{L_1}^2 (Q-B_{L_1})^2$$

$$f_{L_2} = \frac{\pi}{2} F_{L_2}^2 (Q-B_{L_2})^2 \qquad f_{L_3} = 0.$$

That is, the probability of allowed capture is determined by the values of the radial wavefunctions F and G of the captured electron.

To calculate F and G, it is necessary to solve Dirac's equation for the complex potential of an atom. Brysk and Rose (1958) numerically integrated Dirac's equation by representing the radial components graphically as a function of Z and taking into account screening effects and the finite dimensions of the nucleus. Others, including Band and Zyryanova (1958) have since performed the calculation. The results can be found in tables such as those in a book by Zyryanova.

It is the relative capture probabilities that are usually of interest experimentally, since they are independent of the nuclear matrix elements. That is:

$$\frac{W_{L_1}}{W_K} = \frac{G_{L_1}^2}{G_K^2}\left(\frac{Q-B_{L_1}}{Q-B_K}\right)^2 \qquad \frac{W_{L_2}}{W_{L_1}} = \frac{F_{L_2}^2}{G_{L_1}^2}\left(\frac{Q-B_{L_2}}{Q-B_{L_1}}\right)^2$$

and if Q is large, since $B_{L_2} \simeq B_{L_1}$, the second ratio is nearly energy independent. If capture from the M, and higher shells is included, the expression for P_K, which is defined as the ratio of the probability of K-capture to total capture probability, can be written as

$$P_K = \left[1 + \frac{G_{L_1}^2}{G_K^2}\left(\frac{Q-B_{L_1}}{Q-B_K}\right)^2 + \frac{F_{L_2}^2}{G_K^2}\left(\frac{Q-B_{L_2}}{Q-B_K}\right)^2 + \frac{G_{M_1}^2}{G_K^2}\left(\frac{Q-B_{M_1}}{Q-B_K}\right)^2 + \frac{G_{N_{1,0}}^2}{G_K^2}\left(\frac{Q-B_{N_1}}{Q-B_K}\right)^2\right]^{-1}$$

Values for the ratios of the radial wavefunctions, F^2 and G^2, have been tabulated as a function of Z by Zyryanova (1963) and by Robinson (1965). According to these tables, the values relevant to the decay of Osmium are as follows:

$$\frac{G^2_{L_1}}{G^2_K} = 0.1460 \qquad \frac{F^2_{L_2}}{G^2_{L_1}} = 0.06405 \qquad \frac{F^2_{L_2}}{G^2_K} = 0.00935$$

$$\frac{G^2_{M_1}}{G^2_K} = 0.0390 \qquad \frac{G^2_{N_{1,0,\ldots}}}{G^2_{M_1}} = 0.29 \qquad \frac{G^2_{N_{1,0}}}{G^2_K} = 0.01131$$

Using these values, P_K can be calculated as a function of Q.

2.3 Experimental Method to Determine Decay Energy

Something that is of interest in the investigation of β-decay, particularly if $f_o t$ values are to be calculated, is the decay energy. The neutrinos released in the decay process are extremely difficult to detect because of their small interaction cross-section with matter. The energy of the X-rays, which occur when electrons from higher shells cascade down to fill vacancies in lower shells created by the electron capture, is a property of the atomic shells and not of the nucleus. The decay energy cannot therefore, be measured directly by observing the radiations from the decay process. It can, however, in principle, be found from measurements of the ratio of K to L-capture.

One method of determining this ratio involves a coincidence experiment between the K X-rays from the electron capture and the γ-rays emitted from the levels in the daughter nucleus. Consider a simple level scheme as shown below:

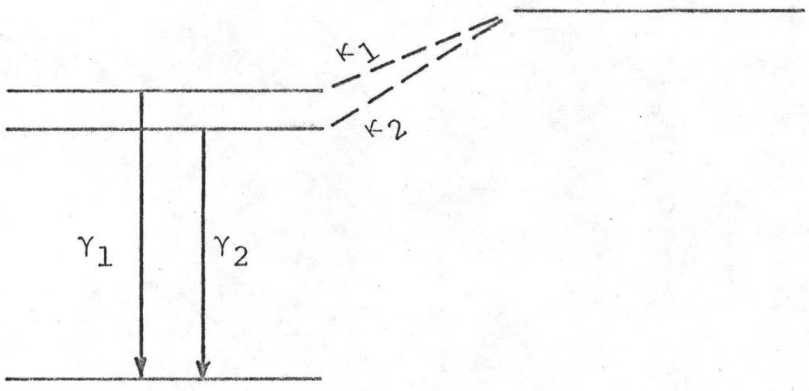

For this case, the number of coincidences observed is given by:

$$N_{\gamma_1\text{-}K} = N_o \kappa_1 b_1 P_{K_1} \omega_K (\varepsilon\omega)_{\gamma_1} (\varepsilon\omega)_K \varepsilon^K_{\gamma_1}$$

where N_o is the source strength, κ_1 is the total electron capture feed to the level, b_1 is the branching from the level, P_{K_1} is the ratio of the probability of K-capture to total capture probability, ω_K is the fluorescent yield, $(\varepsilon\omega)_{\gamma_1}$ and $(\varepsilon\omega)_K$ are the solid angle and efficiency factors for the γ-detector and X-ray detector respectively, and $\varepsilon^K_{\gamma_1}$ is the coincidence efficiency. The number of singles counts for the same gamma transition is given by

$$N_{\gamma_1} = N_o \kappa_1 b_1 (\varepsilon\omega)_{\gamma_1}.$$

The power in the method lies in the fact that by measuring the ratio of $N_{\gamma-K}$ for two different levels and dividing by a ratio of singles, most of the factors above can be cancelled. In particular, no efficiency corrections for the detectors have to be made.

$$\left[\frac{N_{\gamma_1-K}}{N_{\gamma_2-K}}\right] \times \left[\frac{N_{\gamma_2}}{N_{\gamma_1}}\right] = \frac{N_o \kappa_1 b_1 P_{K_1} \omega_K (\varepsilon\omega)_{\gamma_1} (\varepsilon\omega)_K \varepsilon^K_{\gamma_1}}{N_o \kappa_2 b_2 P_{K_2} \omega_K (\varepsilon\omega)_{\gamma_2} (\varepsilon\omega)_K \varepsilon^K_{\gamma_2}} \times \frac{N_o \kappa_2 b_2 (\varepsilon\omega)_{\gamma_2}}{N_o \kappa_1 b_1 (\varepsilon\omega)_{\gamma_1}}$$

If the experimental conditions are adjusted correctly, then it can be safely assumed that $\varepsilon^K_{\gamma_1} = \varepsilon^K_{\gamma_2}$. Therefore

$$\frac{P_{K_1}}{P_{K_2}} = \left[\frac{N_{\gamma_1-K}}{N_{\gamma_2-K}}\right] \times \left[\frac{N_{\gamma_2}}{N_{\gamma_1}}\right]$$

If there is feeding other than electron capture to these levels, correction must be made for coincidences with K X-rays from internal conversion, and with K X-rays from K-capture to the upper level of the cascade.

By comparison of the experimentally determined value of P_K with curves obtained from the calculations shown in 2.2, it is possible to derive the decay energy.

The use of expressions for allowed capture in the case of first forbidden (non-unique) transitions, such as those in the ^{185}Os decay is not strictly valid. The correct expression

for first forbidden (non-unique) capture involves the sum of many terms, each with its own matrix element. The dominant term is that appropriate for allowed capture and algebraic cancellation may be expected among the other terms. Since it is impossible to calculate the small terms with any confidence, it is customary to assume that their effect is negligible and to use only the expression for allowed capture. This approximation is expected to be very good if $Q >> B_K$, but may run into difficulties when $Q \approx B_K$.

CHAPTER III

THE APPARATUS

3.1 Amplification

A Tennelec model TC130 preamplifier, with a very low noise,cooled field-effect transistor as its first stage, and a Tennelec model TC200 double-delay-line linear amplifier were used for amplification and pulse shaping. The TC200 was operated in the single differentiated mode for best resolution. A Nuclear Data ND-502 spectrum stabilizer in conjunction with a Canberra stabilization pulser model 1501 was used to prevent electronic drifts during the accumulation of singles spectra.

3.2 Multichannel Analyzer

This device has the ability to sort out amplified pulses according to the height (that is, according to the energy of the event making the pulse) and to record the relative frequency of occurrence of pulses of different height. Being a multichannel device, the pulse height distribution as a whole can be obtained in a single counting period.

The heart of the device is the analog to digital converter (A.D.C.). In the A.D.C., a capacitor is charged to a voltage which is proportional to the peak voltage of the input

pulse. During the linear discharge of this capacitor, pulses from a periodic pulse generator (in our case a 16 MHz clock) are counted by a scalar; the state of the scalar indicates in digital form the magnitude of the input pulse. The response characteristics of the analyzer are determined primarily by the performance of the A.D.C.

Since radioactive decay is of a random nature, the pulses from the detector are distributed randomly in time. In order that only one pulse occurs in the converter circuit during analysis, there is a linear gate which closes during the analysis time required for the pulses already in the converter and which opens when the analysis is complete.

Since the time required for analysis depends upon the address assigned to the pulse, the overall dead time for a particular counting period depends upon the nature of the spectrum involved. The actual live time of the analyzer during a given counting period is measured by scaling a clock oscillator.

The analyzer used was a Nuclear Data 161 4096 channel analyzer, each channel being able to contain an 18 bit word corresponding to a maximum count of 262,144.

3.3 Coincidence Technique

(a) Electronics:

The gamma-gamma coincidence measurements were carried out with the above analyzer, but in a two parameter configuration.

A block diagram of the circuit used is shown in figure 1.

The TC 200's were adjusted to give double differentiated pulses; these were fed to a timing single channel analyzer (Canberra model 1435) on the NaI(Tl) side, and to a zero strobe (Canberra model 1421) on the Ge(Li) side. These units were both operated as zero strobes; that is, they detected the zero crossing point of the bipolar pulses and generated a timing signal when the input pulse crossed the zero voltage baseline. Crossover timing rather than leading edge timing was used in order to minimize walk.

These timing pulses were then routed to a fast coincidence unit (Canberra model 1440) which generated a rectangular logic pulse whenever the two pulses arrived within the adjustable resolving time of the zero strobes. A second set of timing pulses, one arbitrarily delayed with respect to the other, was routed to another fast coincidence unit. Negative pulses were fed to a scalar from each fast coincidence unit. The output from the first gave true + chance coincidences, the second (delayed) giving chance coincidences. The ratio of the counts accumulated in these two scalars gave the (true+chance)/chance ratio for the experiment. From the fast coincidence unit, positive logic pulses were fed to the coincidence inputs of the analyzer, enabling it to accept the two coincident pulses from the detectors.

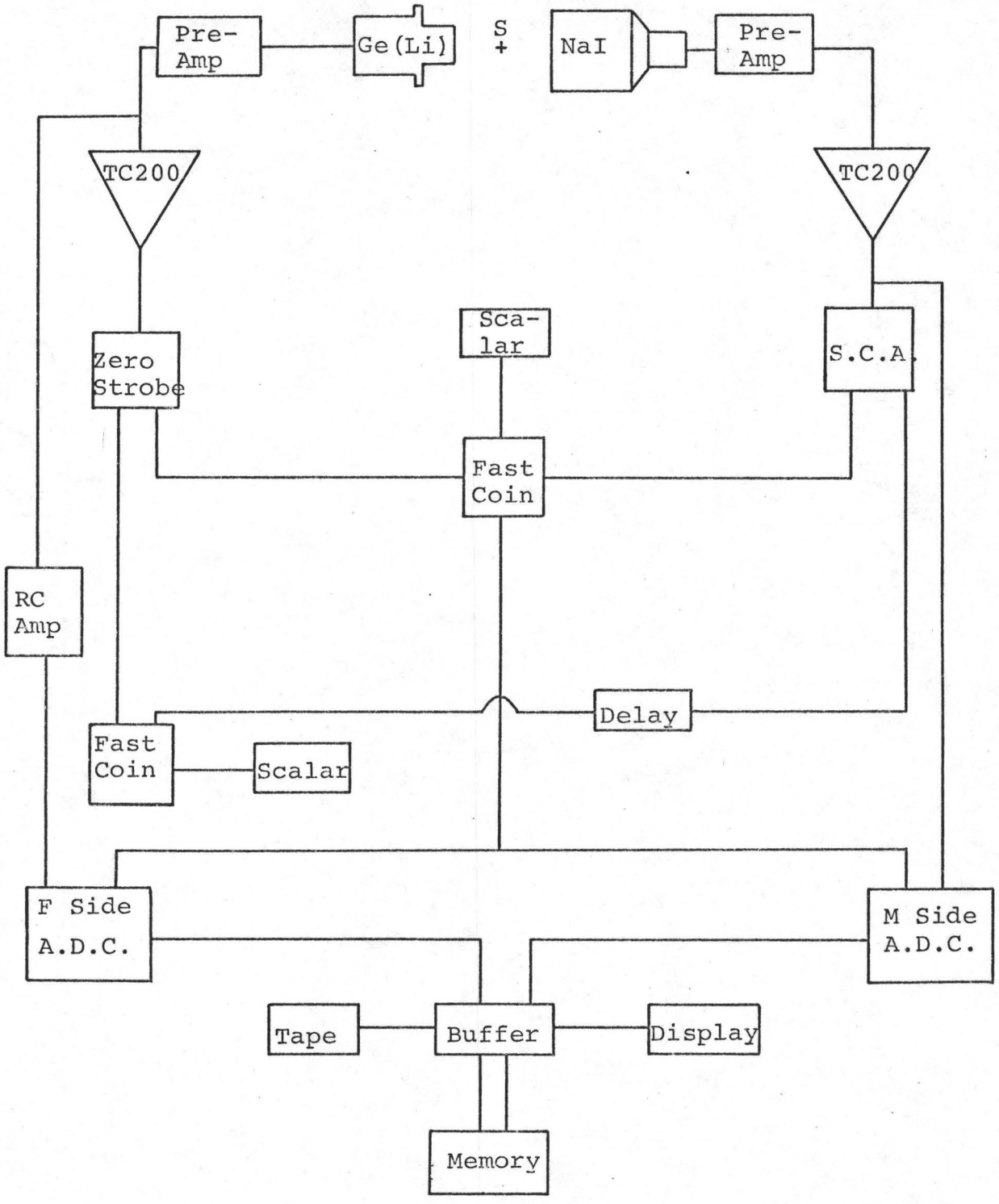

FIGURE 1

TWO DIMENSIONAL COINCIDENCE SPECTROMETER.

(b) Data Handling and Analysis:

When used in a two-parameter configuration, the memory of the analyzer is divided into two sections: one for oscilloscope display, the other for storage. The data from the coincidence experiment was recorded in a 256(NaI) × 1024(Ge(Li)) channel matrix. This large matrix was achieved by address-recording each event on magnetic tape. When a coincident event is detected, the information from the Ge(Li) detector is written in a 10-bit word and the information from the NaI detector in an 8-bit word; these combine to form one of the 18-bit locations in the memory. Each event was then placed in matrix position (i,j), where channel i was proportional to the pulse height from crystal 1 and channel j was proportional to the pulse height received from crystal 2. Each event is stored sequentially. When the storage half of the memory contains 2048 coincident events, the information is dumped automatically onto magnetic tape and then counting is continued. A single data tape contained approximately 1.8×10^6 events.

These events were sorted at a later time into the desired matrix with the University IBM 7040 computer. Since the size of the 256 × 1024 matrix is too big for the computer memory to handle at one time, the matrix is divided into eight 256 × 128 submatrices. The computer checks the data tape and places appropriate events into the proper place in the first submatrix. After a complete pass through the data tape, the

contents of the memory are dumped onto a second tape. Then, a second pass through the data tape is begun to place events in the second submatrix. Eight passes are needed to sort the data tape.

(c) The Problem of Chance:

As well as true events, a number of chance events, which are due to the finite resolving time of the detector, are recorded. Consider a simple cascade: The counting rate in one detector is given by $N_1 = N_o\varepsilon_1\omega_1$ and that in the other by $N_2 = N_o\varepsilon_2\omega_2$. N_o is the source strength, ε_i is the detector efficiency and ω_i is the solid angle. The true γ-γ coincidence rate will be given by $N_{12} = N_o\varepsilon_1\omega_1\varepsilon_2\omega_2$. The chance rate, if each detector accepts events for a time τ, is given by $N_{ch} = 2\tau N_1 N_2$. The ratio of true to chance coincidence will therefore be $N_{12}/N_{ch} = 1/2\tau N_o$. Thus, if the true to chance ratio is to be as large as possible, τ which is determined by the apparatus should be short and N_o should be small. Usually, a compromise must be made. If τ is made too short, a loss of coincidence events results. Also, the coincidence efficiency will not be a constant for the entire energy spectrum. If N_o is made too small, there will be few coincidence events. In more complex

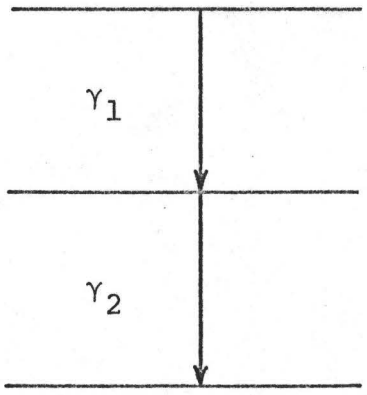

decay mechanisms, the above simple formula is no longer adequate but the general result displays the same type of dependence on N_o and τ.

The chance spectrum has the same shape as the singles. Correction for chance can be made by summing the coincidence projection, finding the number of chance counts by dividing this by the experimentally measured true/chance ratio, and then normalizing the singles spectra to this value.

3.4 Chalk River $\pi\sqrt{2}$ Spectrometer

For the interpretation of nuclear disintegration schemes, two criteria are needed for the experimental apparatus: high resolving power and high precision (that is, relative accuracy). For the internal conversion process, the interpretation of conversion line spectra is often quite ambiguous without adequate resolution. Also, high resolving power enables one to identify uniquely the multipolarity of a given transition from a comparison of the experimental internal conversion line intensity ratios $K:L_1:L_2:L_3$ with the theoretically predicted ratios.

The Chalk River Spectrometer (Graham, Ewan and Geiger 1960) is a one-meter radius, iron-free double-focussing $\pi\sqrt{2}$ spectrometer. It is designed to have a resolution of from 0.01% to 1% full line width at half maximum depending on the transmission aperture, which can be adjusted from 0.1% to 1.0% of 4π

steradians. Since the spectrometer is of air-cored design, the magnetic field strength, and hence the momentum of the focused electrons is directly proportional to the excitation current in the coils, which can be measured with high precision using standard methods.

The precision with which momentum focused monoenergetic electrons can be measured using this spectrometer depends primarily on the precision with which the current through the coils can be controlled and measured. The spectrometer current stabilizer was designed to ensure that the proportionality between the momentum of the focused electrons and the current in the coils was constant over the useful momentum range to better than 1 part in 10^5. The eight spectrometer coils are all connected in series and the current is derived from a 600 volt 50 ampere d.c. generator. The current is regulated by comparison of the RI drop across one of a set of standard resistors with a reference potential.

The preselected reference potentials for the experiments were created by a stepping potentiometer. It could be programmed to give up to 1,000 equally spaced reference voltages in sequence, starting at any desired zero-position voltage, V_o, in the range 0 to 1 volt. The magnitude of the primary voltage increments, ΔV, are independent of V_o and can be set to any of a variety of values in the range 5 to 1,000 microvolts. With this stepping reference potentiometer in operation, the

current settings were checked at the end of every other counting period. The RI drop across the standard resistor was measured using an independent precision potentiometer, which is standardized against one of a pair of saturated standard cells in a constant temperature enclosure. At the end of each counting period, usually 40 seconds, the index number of the stepping potentiometer and the counts accumulated in the scalar were typed out. The stepping potentiometer was then advanced to the next current setting, the scalars reset and the counting restarted. The stepping potentiometer could be programmed to recommence the sequence of current settings after any desired decade of increments.

If the conversion lines being sought are weak in intensity, and if there is a problem of background, an alternative procedure can be used to scan the conversion lines. This procedure involved the use of a 400 channel Victoreen analyzer. As before, the start position for the scan was set by the stepping reference potentiometer. Now, the upper end of the scan was set by means of another potentiometer which was coupled to the Victoreen. By means of suitable adjustments, one was able to place the region of interest within the 400 channels of the analyzer. As before, the system advanced automatically, and repeated the scanning cycle until stopped. The advantage of the system is that 1/4 second of counting time is taken at each current setting, with the result that

background fluctuations are minimized. The system typed out the total number of counts received in any particular current sequence; at the end of a run, the 400 channel contents of the analyzer are printed out. Current readings are taken at the beginning and end of the run, and periodically during the run.

With the detector arrangement in the spectrometer, it was possible to interchange the detector window. With a thin Mylar window (~ 1 mg/cm^2), the unit is operated as a flow-type proportional counter with an atmospheric pressure methane filling. Due to the fact that low energy electrons (<100 keV) were absorbed in this window, a thinner window had to be used for the low energy conversion lines. A laminated film (~ 100 μg/cm^2), prepared by superimposing 10 to 20 layers of VYNS plastic films, served as the thin window. It was supported by a fine-mesh metallic grid of ~ 90% open area. The filling pressure for this counter is of the order of a few cm. of Hg. This thin window technique makes it possible to measure the relative intensities of conversion lines down to ~ 20 keV. The reduced stopping power of the low pressure gas filling does, however, reduce the efficiency for energetic electrons, some of which can traverse the counter without creating one ion pair. For this reason, the thin window counter was not used above 100 keV. Intercalibrations were made between the two window systems to relate the intensities of the low and high energy conversion lines.

CHAPTER IV

PREVIOUS AND CONCURRENT INVESTIGATIONS

4.1 Survey of Previous Work

The experiments of Goodman and Pool (1947) and Katzin and Poberskin (1948) established that ^{185}Os decayed by orbital electron capture to ^{185}Re with a half life of 94 days. Since then many workers, including Bunker et al (1950), Swan et al (1952), and Cork et al (1953) have investigated this decay. Miller and Wilkinson (1951) showed that L-capture occurred in a significant fraction of the disintegrations.

When the present investigation was undertaken, the decay scheme was essentially that due to Johns et al (1957). The internal and external conversion spectra associated with the decay of ^{185}Os were studied with a 50 cm Siegbahn type β-ray spectrometer adjusted to an instrumental resolution of 0.65% in momentum. Gamma-gamma and gamma-X-ray coincidence experiments were also carried out using NaI(Tl) detectors. The decay energy was measured from the ratio of L-capture to K-capture to the 872 and 879-keV levels. The decay scheme constructed on the basis of these investigations is shown in figure 2.

The Decay Scheme of Johns et al

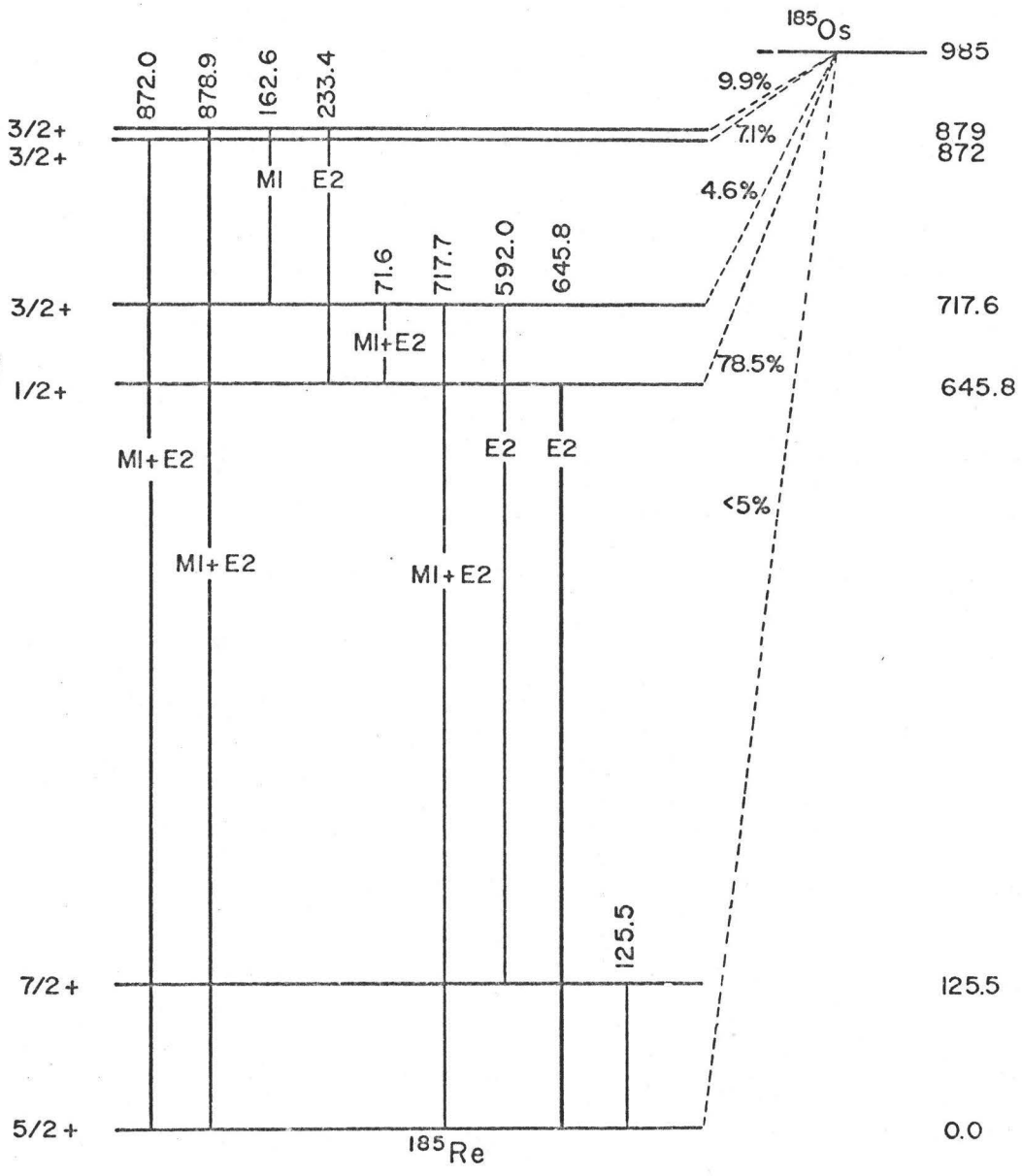

Figure 2

4.2 Initial Aims of the Present Investigation

The present investigation was begun with the intention of conducting a search with a Ge(Li) detector for weak radiations that might exist in the ^{185}Os decay, but which were not found in the previous experiments. The improved resolution of the Ge(Li) detector meant that the chances of finding any existing weak radiations were good. Also, a check of the energies and intensities of the known γ-rays, unresolved in previous work, would be carried out. In particular, a search was to be made to look for transitions to the 125-keV level from the 872 and 879-keV levels, and for transitions from the 872-keV level to the 646 and 717-keV levels. If the spin assignments of Johns et al were correct, these transitions should compete favourably with the existing transitions.

The decay energy was to be remeasured with a K X-ray-gamma ray coincidence experiment, and a gamma-gamma coincidence experiment was to be performed to confirm the existing decay scheme.

4.3 Work Concurrent to the Present Investigation

During the course of these investigations, a paper was published by Metzger (1967), in which he observed resonant scattering of γ-rays from the 646, 717 and 874-keV excited states with NaI as well as Ge(Li) detectors, and measured the angular distributions of the resonance radiations. An ^{185}Os

source, moving on the periphery of a fast rotor at speeds of up to 1.3×10^5 cm/sec, provided the resonant γ-rays. From the magnitude of the scattered effects and from the known spins, which were verified by the angular distribution measurements, the transition probabilities and B(E2)'s were determined for the ground state transitions. In a measurement of the high energy portion of the direct gamma ray spectrum, he noted the presence of a 929 ± 2 keV transition and on a half-life basis, tentatively assigned it to the ^{185}Os decay as a ground state transition.

Also,during this time, a paper was published by Schulz (1967), in which he measured P_L/P_K electron capture ratios to the 873+878 keV level and P_L/P_K and P_M/P_L capture ratios for the 646-keV level. From these, a value of 1010 ± 4 keV was deduced for the decay energy. All measurements were done with scintillation crystals containing the radioactive nucleus as a constituent of the crystal lattice. Furthermore, the existence of a 5-keV transition between the 878 and 873-keV levels was proposed. A transition intensity of 4.1% was assigned to it.

4.4 Revised Aims

Due to the results of the experiments described in 4.3 and to the preliminary results of the present investigation, several new aims were resolved. The nature of the 929-keV transition was to be investigated and an effort made to firmly

place it in the decay scheme. Also, a second measurement of the decay energy was to be performed, in which K-capture to the 929 level would be looked for.

CHAPTER V

THE EXPERIMENTS

5.1 The Ge(Li) Gamma Ray Singles Measurements

The majority of the gamma singles experiments were done with a planar type Ge(Li) detector from Nuclear Diodes. Its area was 1.5 cm^2 and its depletion depth 0.4 cms. giving an active volume of 0.6 cm^3. The resolution (full width at half maximum) of the whole system ranged from 1.8 to 2.3 keV at 100 keV during the runs. Two reproducible geometries were used when counting. In one, the source was placed 4 cm. from the detector can and no absorber was used. For the other, the source was placed at the same distance, but an absorber was placed between the detector and the source. The absorber consisted of two thin sheets of lead (~ 1 mm) and two thin sheets of cadmium (~ 1 mm), the cadmium being on the detector side of the lead. The lead served the purpose of absorbing the rhenium X-rays produced from electron capture and internal conversion; the cadmium absorbed the lead X-rays.

Preliminary measurements involved a source of natural osmium metal containing 0.018% ^{184}Os. Irradiations were made in the McMaster reactor with 10 mg of material sealed in a quartz capsule and irradiated in a flux ~ 10^{13} $n/cm^2/sec$ for a period of 10 days. This was followed by a cooling period of three weeks to allow the large amount of ^{193}Os (33 hr.)

formed in the irradiation to decay. The presence of several of the stronger radiations from ^{192}Ir (74 days) indicated the need for a chemical purification. Furthermore, the 129-keV gamma ray from ^{191}Os, which completely obscured the 125-keV gamma ray from ^{185}Os, indicated the need for an enriched source. In both cases, the half-lives of the impurities, being comparable to that of ^{185}Os, made it impossible to wait for them to decay.

Subsequent irradiations involved 1 mg of osmium metal, enriched to 2.5% in ^{184}Os, sealed in a quartz capsule and irradiated for a period of 10 days in the Chalk River NRX Research Reactor at a flux ~ 10^{14} n/cm^2/sec.

Gamma singles experiments were subsequently done using two Ge(Li) detectors at Chalk River. In order to improve the statistics of the high energy part of the spectrum, an intensity run with ~ 3 mm of Pb and Cd absorber was made with a 30 c.c. Ge(Li) detector. Since a number of clean-up drifts had been made on our detector, another singles run was performed on a 1 c.c. detector of 2 keV resolution at 660 keV to check the intensity relationship between the high and low energy portions of the spectrum.

Typical counting runs at McMaster averaged 72 hours, the longest being 150 hours in a geometry with absorber.

5.2 Efficiency and Energy Calibration

In order to determine the relative intensities of the gamma rays in the spectrum, it was necessary to measure the efficiency of the Ge(Li) detector as a function of energy. The photopeak detection efficiency of the Ge(Li) crystal for the geometry without absorber was measured using an efficiency curve determined by other members of the group. The curve was determined by using a number of standard sources: ^{241}Am, ^{203}Hg, ^{139}Ce, ^{203}Hg, ^{51}Cr, ^{198}Au, ^{22}Na, ^{207}Bi, ^{137}Cs, ^{54}Mn, ^{60}Co. The source strengths were measured using a NaI(Tl) detector and the tabulated efficiencies and photofractions of Heath (1964). The result is shown in figure 3. The photopeak efficiency for the geometry with absorber was determined using a ^{152}Eu source with the relative intensities of gamma lines as given by Dzhelepov et al (1966). The result is shown in figure 4. For the Chalk River gamma runs, the photopeak efficiency was taken from their curves.

Energies were determined using a multiple source technique; that is, spectra were taken of a sample of ^{185}Os along with several calibration sources. Calibration sources used were ^{141}Ce, ^{51}Cr, ^{198}Au, ^{22}Na, ^{137}Cs, ^{56}Mn, ^{46}Sc. Correction for the non-linearity of the detecting system, particularly the A.D.C., was determined using a non-linearity curve measured by other members of the group. The non-linearity was determined as follows. The peak positions of a large number of calibration

FIGURE 3

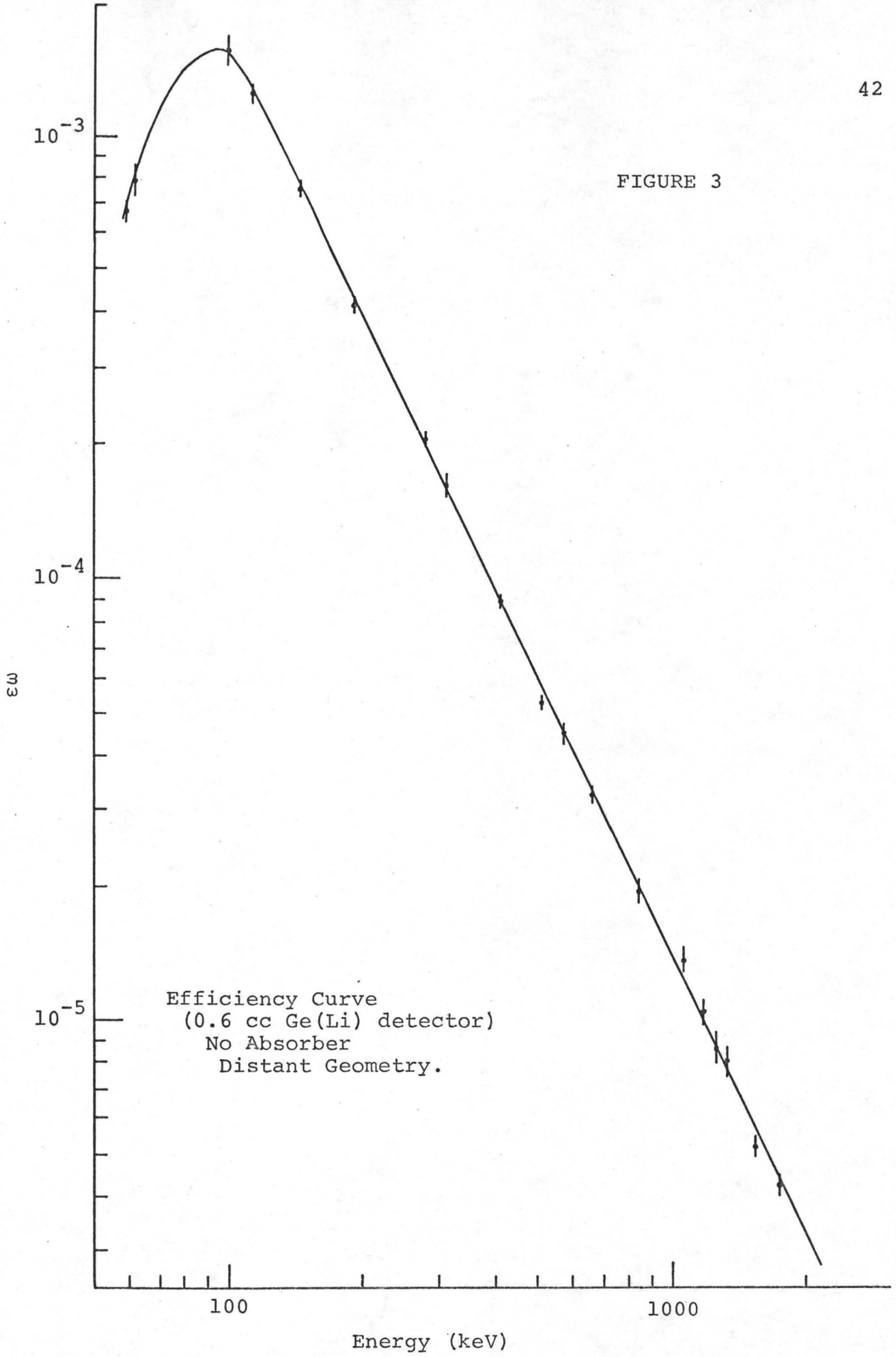
10^{-3}
10^{-4}
10^{-5}
εω
Efficiency Curve
(0.6 cc Ge(Li) detector)
No Absorber
Distant Geometry.
100
1000
Energy (keV)

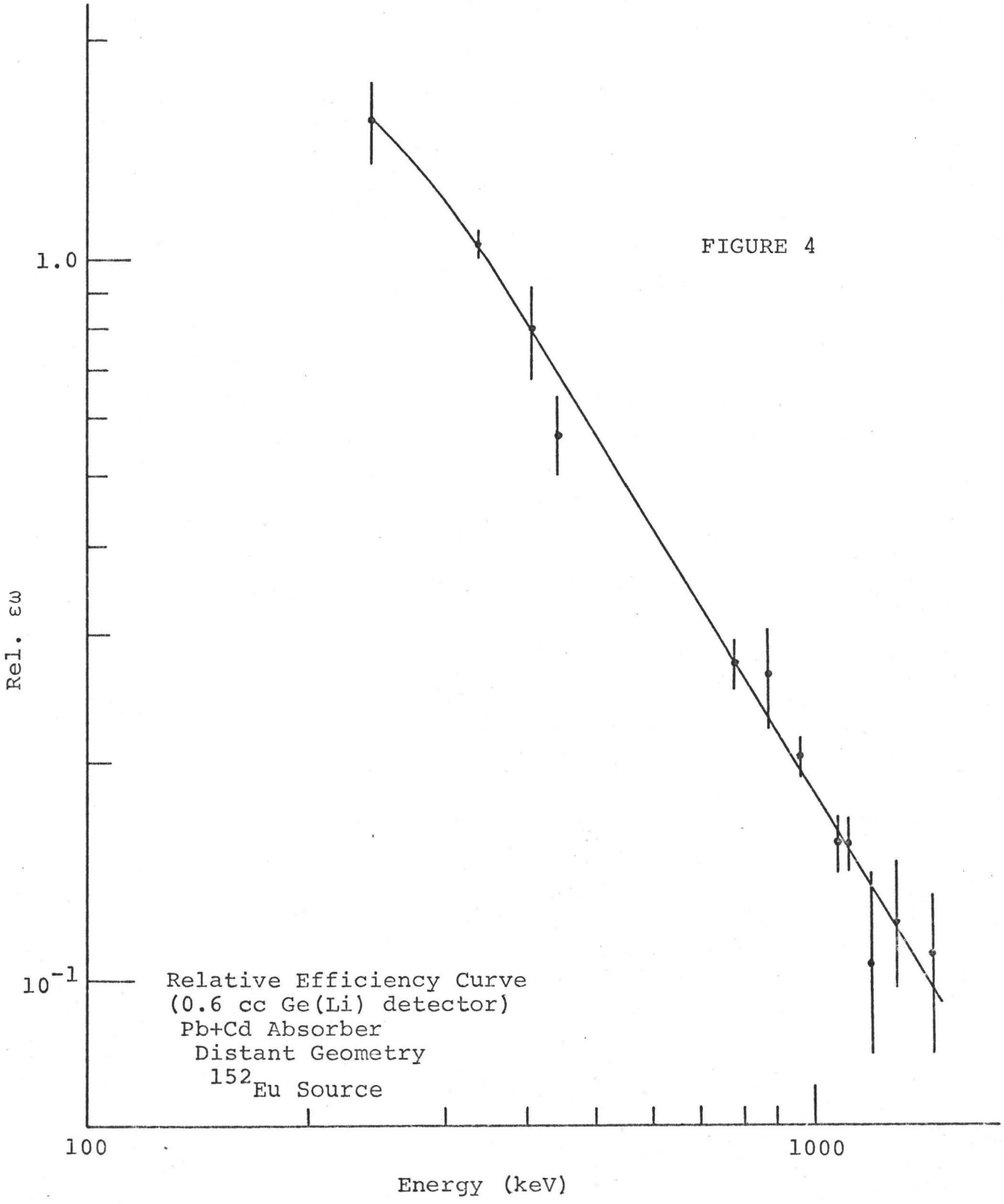
1.0
10^{-1}
Rel. εω
Relative Efficiency Curve
(0.6 cc Ge(Li) detector)
Pb+Cd Absorber
Distant Geometry
^{152}Eu Source
100
1000
Energy (keV)

FIGURE 4

sources were accurately determined. Two of these (the 511 and 1274 lines of ^{22}Na) were arbitrarily chosen to have zero non-linearity correction and then corrected peak positions were found by comparison of the observed values and the calculated values. The overall departure from linearity between channels 400 and 3500 was less than 1-1/2 channels.

5.3 Chemistry and Electroplating

The presence of the small amounts of iridium impurity mentioned in 5.1 were removed by means of the chemical purification procedure described below. Also since beta-sources were needed, a plating procedure is described.

The osmium metal was dissolved in a solution of aqua regia (the quartz capsule being broken under the solution). The resulting solution was heated slowly and the osmium distilled over into a solution of 5% H_2O_2. (If heat is applied too vigorously, the nitric acid just boils off and leaves the osmium behind). A drop of H_2SO_4 was added to the active solution which was then distilled into a 20% NaOH solution. As this distillation proceeds, the NaOH solution turns yellow. Heat must be applied rather gently since it is easily possible to drive the osmium over so quickly that it is not trapped in the NaOH but proceeds up the fume hood exhaust.

The NaOH solution solution containing the active osmium, plus an equal amount of plating solution (4 parts

ammonium phosphate + 18 parts sodium phosphate + 1 part sodium chloride) is then put into the plating cell. The cell is shown below. A platinum wire provides the anode; the

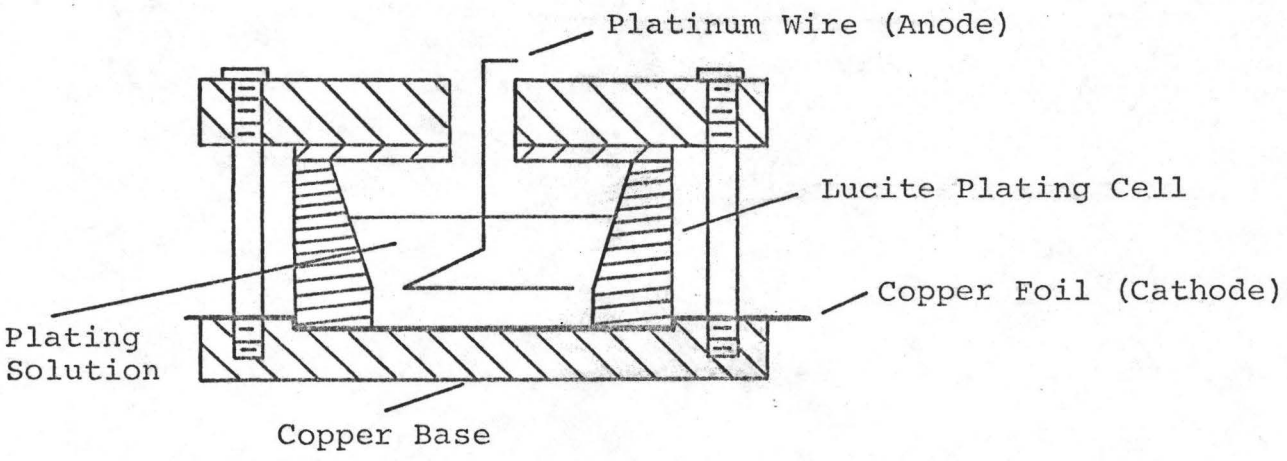

copper foil (4.6 mg/cm^2) on which the source is to be plated provides the cathode. The plating was done at 200 ma. The time of plating depended on the specific activity of the source, on the strength of the beta source desired, and the source thickness that could be tolerated. Typical sources measured 3 cm. long by 3 mm wide and typical plating times were 20 minutes.

5.4 Chalk River $\pi\sqrt{2}$ Internal Conversion Measurements

The internal conversion study was carried out using the Chalk River precision iron-free $\pi\sqrt{2}$ beta spectrometer described in Chapter III. Three runs of different baffle settings, source widths and counter defining slits were made.

The following table shows the peaks investigated:

Baffle Settings	Source Widths	Counter Slit Widths	Peaks Investigated
0.05%	2 mm	2 mm	^{198}Au 411 K; 646 K, L's; 875 K; 880 K .
0.15%	3 mm	3 mm	71 L's; 125 K, L's; 163 K, L's; 234 K, L's; 646 K, 717 K.
0.07%	3 mm	5 mm	71 L's, M's; 125 K, L's; 163 K; 234 L's; ^{198}Au 411 K; 592 K; 592 K; 646 K, L's; 875 K; 880 K.

For the first and third runs, the 411 K peak of ^{198}Au was used as a standard for the Bρ calibration. The calibration involved the average of two determinations of the peak position in μV (the second involved the source in an inverted position with respect to the first). In this way, readings taken in μVolts were related to the known Bρ value of the Au line. For the second run, the 646 K peak was used as an internal calibration standard. Since all electron intensities were to be normalized to the 646 K peak, it was repeated at each resolution setting.

Due to the fact that the ^{185}Os decay is by electron capture, there is no β-continuum to contribute to the background. Therefore, the background should essentially be that due to γ-rays producing Compton electrons that are detected in the counter. However, there is a fluctuating contribution to the

counter background arising from the 1.3 MeV γ-ray of ^{41}Ar which is created by neutron activation of the cooling air which flows through the NRX and NRU Research Reactors and is ventilated to the atmosphere. The effect of the ^{41}Ar γ-rays depends upon the atmospheric conditions. The normal counter background rate (≈ 40 cpm) could easily be increased by a factor of 10 by the ^{41}Ar. In fact it was this background that was the most important factor in assigning line intensity errors and which was the limiting factor in searches for weak lines.

Except for the 646 K and the 411 K (^{198}Au), which were done by the stepping procedure described in Chapter III, all the other peaks were scanned by means of the Victoreen system explained in Chapter III. Because of the fluctuating background described above, a system had to be used in which the counting time per momentum setting was short compared to the background fluctuations. Typical runs on the Victoreen system took 15 to 18 hours.

Due to the fact that low energy electrons (< 100 keV) were absorbed by the normal window on the proportional counter used to detect the electrons, a special thin window had to be used for the low energy conversion peaks. The counter arrangement is described in Chapter III. A counter intercalibration was made using the 163 K line to relate the low and high energy intensities.

5.5 Si(Li) Internal Conversion Measurements

The internal conversion spectrum was also measured using a Kevex Si(Li) detector cooled to liquid nitrogen temperatures. Its area was 80 mm^2 and its depletion depth was 3 mm. The resolution (full width at half maximum) was 4.7 keV at 650 keV. A Canberra 1408C preamplifier was used with the system described in Chapter III. The electron conversion peak efficiency of the Si detector was calibrated using the relative number of electrons determined in the $\pi\sqrt{2}$ internal conversion measurements. Although the resolution of the above detector was not good enough to separate the 931 K from the 875-880 L's, the experiment was performed in the hope of finding the 931 L peak. A 72 hour run was made.

5.6 Ge(Li)-NaI(Tl) Coincidence Experiment

The 2-parameter gamma-gamma coincidence experiment was carried out with a 0.6 cc Ge(Li) detector which gave a resolution of 3 keV at 200 keV, and a 3" x 3" NaI(Tl) detector in coincidence. A 180° geometry was tried initially, but the Compton scattered radiation dominated the counting rate. A 90° geometry could not be used because of the very low counting rate. A compromise of a 120° geometry was used; this reduced the Comptons substantially, but still gave a reasonable coincidence counting rate. The source was placed in a hole in an anti-Compton shield; the shield was placed as shown below. Three

sheets of Cd (~ 2 mm) were placed in front of the NaI detector to absorb the Re X-rays in order to reduce the counting rate in the NaI detector. A resolving time of 100 nsecs was used.

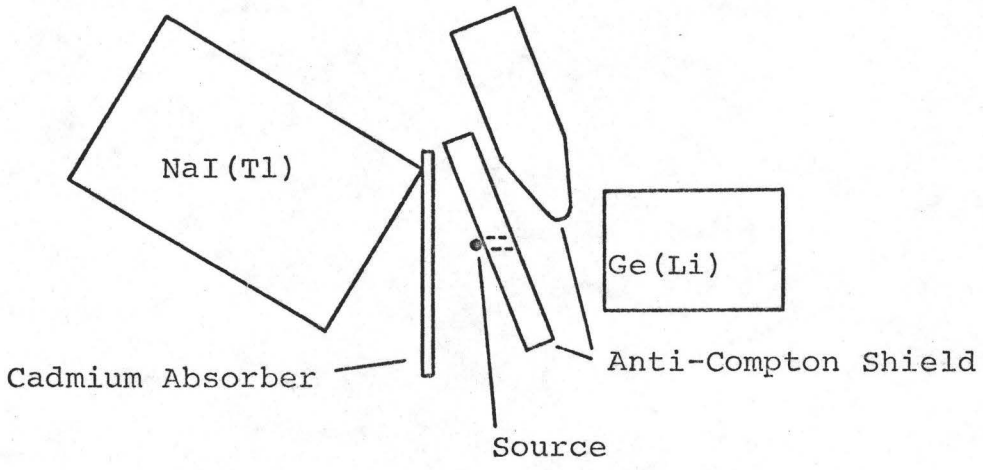

5.7 The Decay Energy Measurements

A 2-parameter K X-ray gamma coincidence experiment was performed to determine the decay energy according to the method described in Chapter II. The X-ray detector was a 15/16" diameter by 1/8" thick NaI(Tl) detector with a thin Be window. The gamma-ray detector was an 8 cc Ge(Li) detector with a resolution of ~ 6 keV at 1100 keV. The experiment was performed in a 180° close-up geometry; a large amount of Pb and Cd absorber (~ 8 mm) was used in front of the Ge detector to absorb most of the low energy radiations (< 150 keV). The window width of the single channel analyzer on the NaI side was adjusted to generate logic pulses only if the analog pulses from the amplifier corresponded to energies less than 100 keV. Since X-rays were the only radiation of interest

on the NaI side, this was done to reduce the counting rate in the NaI detector. A resolving time of 75 nsecs was used.

In the first run (true/chance ratio of 30:1), two data tapes were accumulated. A second run was performed over a two and a half week period, in which the discriminator setting on the zero strobe on the Ge side was adjusted to generate logic pulses only if analog pulses from the amplifier correspond to energies greater than 670 keV. This was done to eliminate coincidence events due to 646-keV γ - K X-ray coincidences which were accounting for nearly all the coincidence events being recorded on tape. The true/chance ratio throughout the run was 36:1. Singles (self-coincidence) spectra for both detectors were taken in each experimental configuration.

CHAPTER VI
RESULTS

6.1 Gamma Ray Measurements

Intensity runs were taken in each of the geometries described in Chapter V. The intensities, relative to the strong 646-keV transition, were found through the use of an appropriate efficiency curve (see Chapter V) by determining the number of counts in the peak between X_o-3F and X_o+2F, where X_o is the peak position and F is the half width at half maximum. The same criterion was used in determining the efficiency curve measured by this worker. To first order, the relative efficiency curves should be independent of the criterion used for determining the peak area. This was shown to be so by the fact that the efficiency curves obtained for the same detector by other workers in the lab gave consistent results with the present determination, despite the fact that each worker used a slightly different criterion for the peak area. The energies were determined from the peak positions using the procedure described in Chapter V and are the weighted average of several runs. In each case, data was accumulated in the buffer storage and dumped onto magnetic tape at regular intervals during the run.

Figure 5 shows two portions of the gamma ray spectrum. The low energy portion is taken from a geometry without absorber

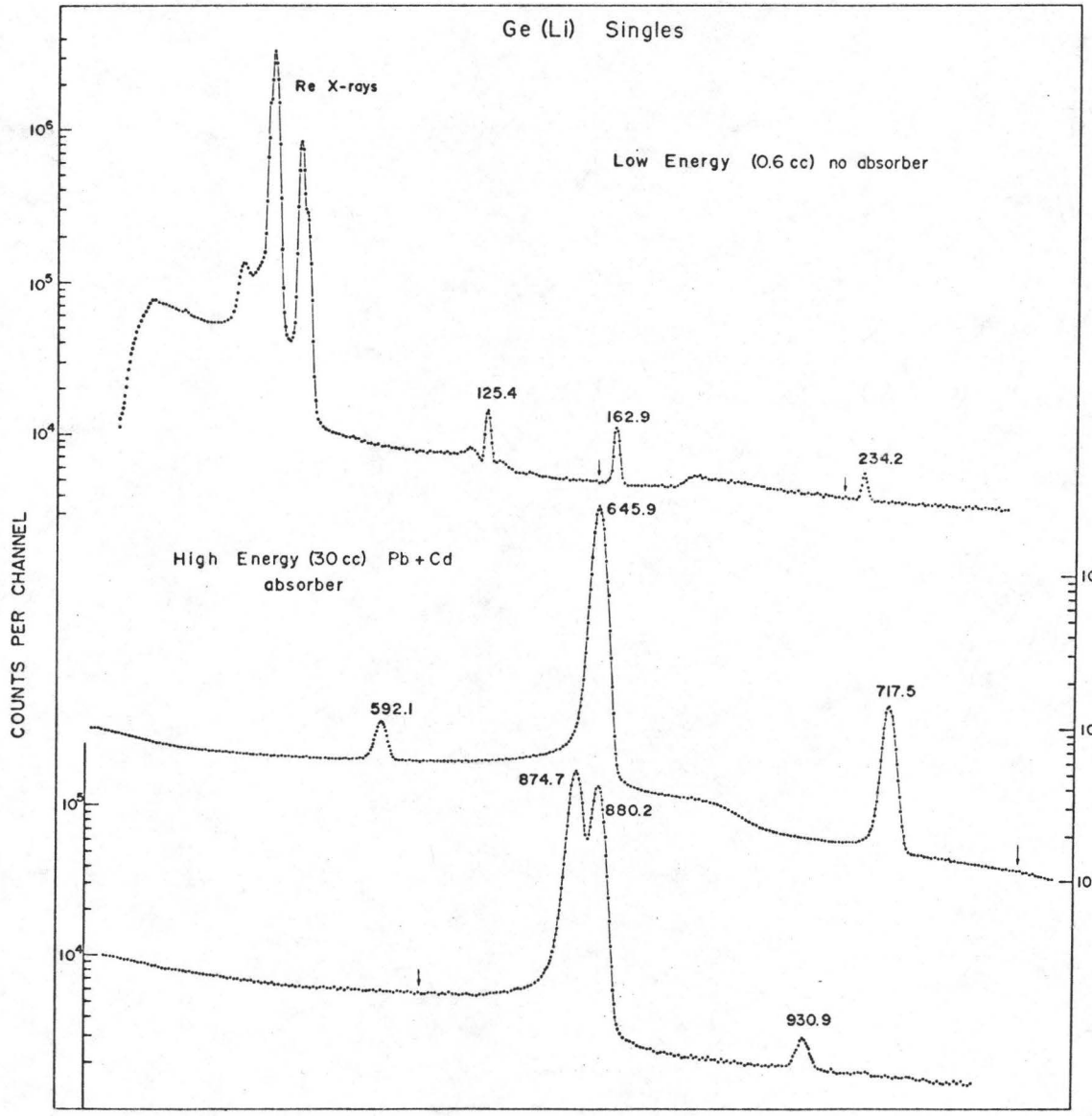
Ge (Li) Singles
Re X-rays
Low Energy (0.6 cc) no absorber
125.4
162.9
234.2
645.9
High Energy (30 cc) Pb + Cd
absorber
592.1
717.5
874.7
880.2
930.9
COUNTS PER CHANNEL
10^6
10^5
10^4

Figure 5

measurement, the high energy portion was obtained with a lead plus cadmium absorber. Arrows indicate where the peaks of the possible 158, 229, 749 and 836-keV transitions would be found. The weighted averages of these measurements and the Chalk River runs are compared with those of Johns et al, and Metzger and are presented in Table I.

As seen from the table, the agreement between the present work and that of Metzger's is quite good for the higher energy portion of the spectrum. The energy separation of the 875, 880-keV doublet was found to be 5.5 ± 0.2 keV. For the ratio of the two intensities, a value of $\frac{I_{875}}{I_{880}} = 1.25 \pm 0.03$ was found, in good agreement with Metzger's value of 1.18 ± 0.06. The intensity of the weak 931-keV transition, seen by Metzger, was also confirmed. Upper limits of $\simeq$ 3% of the 163 and 234-keV transitions from the 880-keV level to the 717 and 646-keV levels respectively were set on the existence of corresponding transitions from the 875-keV level to the 717 and 646-keV levels. Upper limits of 0.012 and 0.007 respectively (per 100 decays) were set on the existence of a 749-keV transition from the 875-keV level to the 125-keV level and on the ground state transition from the 836-keV level seen in inelastic scattering experiments by Bisgård and Veje (1967). On comparison of the present work with that of Johns et al, it is interesting to note the discrepancy in the intensity of the 234-keV line; the new intensity is a factor of three greater than the old value.

TABLE I

Gamma Rays in the Decay of ^{185}Os

Transition (keV)	Present Work		Johns et al		Metzger	
	Energy(keV)	Intensity[a]	Energy(keV)	Intensity[a]	Energy(keV)	Intensity[a]
K X-rays	K X-rays	67.5 ±6.1	K X-rays	66.6 ±7.3	...	...
717 → 646	71.4[b]	0.11±0.03[b]	71.6±0.3	...	...	...
125 → 0	125.4±0.3	0.40±0.06	125.5±0.4	0.65±0.3	...	...
875 → 717	157	<0.016	...	...	...	...
880 → 717	162.9±0.2	0.72±0.07	162.6±0.2	0.65±0.3	...	...
875 → 646	229	<0.016	...	...	...	...
880 → 646	234.2±0.2	0.45±0.065	233.4±0.6	1.2 ±0.3	...	...
717 → 125	592.1±0.3	1.2 ±0.1	592.0±0.4	1.1 ±0.2	592	1.1
646 → 0	645.9±0.2	81.3	645.8±0.3	81.3	645.9±0.5	81.3
717 → 0	717.5±0.2	4.0 ±0.3	717.7±0.5	4.1 ±0.4	717.8±0.5	3.6
875 → 125	749	<0.012	...	...	749	<0.012
836 → 0	836	<0.007	...	...	836	<0.016
875 → 0	874.7±0.3	6.9±0.6	872.0±1.5	7.2 ±0.5	874.0±0.5	6.6
880 → 0	880.2±0.3	5.5±0.5	878.9±1.0	7.6 ±0.5	879.4±0.5	5.5
931 → 0	930.9±0.5	0.05±0.009	...	...	929 ± 2	0.05±0.009

a) per 100 decays b) from the L-shell conversion lines

This is not surprising, since the energy dependence of the efficiency for the external conversion technique using the magnetic spectrometer was very poorly known at the time of these measurements.

6.2 $\pi\sqrt{2}$ Internal Conversion Results

The area of the conversion lines was determined by summing the total counts, which were taken at equally spaced momentum intervals, over the region of the conversion line in question. From this was subtracted the contribution due to background. The net difference multiplied by the momentum increment used in the scan and divided by the momentum assigned to the line gives the required "area".

The line shape observed is asymmetrical with a low energy tail, partly because of the focussing properties of the spectrometer and partly because of the energy degradation in the finite surface density of the source deposit. The former is a constant of the instrument and independent of the electron momentum. The momentum setting for each conversion line was deduced from the centre of the top of the peak rather than from the peak centroid or from a linear extrapolation of the high energy side down to the continuum. This empirical procedure is nearly independent of natural width effects and appears to be relatively insensitive to energy degradation in the source (Geiger, Graham and Ewan 1960). The mid-point of the line is determined at several heights and a line passing

through these mid-points is then taken as the momentum settings assigned to the line.

The conversion peaks are shown in Figures 6 and 7. The energies, intensities and multipolarities derived from the $\pi\sqrt{2}$ internal conversion measurements are shown in Table II. The energies and intensities are the weighted averages of several runs taken at different momentum resolution settings. The intensities have been normalized in such a way as to represent the number of conversion electrons per 100 decays. The basis for this normalization is described below. Wherever possible, the L subshell ratios were used to determine the mixing ratio. The photon and electron intensity scales were then related through the K-conversion intensity of the 646-keV transition which, from the L subshell ratios, appears to be pure E2. With this normalization, the values of α_K for the other transitions were found, as tabulated in column 4. It is seen that the multipolarities deduced from these agree quite well with those found from the L subshell ratios. The theoretical conversion coefficients were taken from the tables of Sliv and Band found in Vol. II of Siegbahn (1965).

The multipolarities of the 646 (E2), 592 (E2), 163 (M1) and 125 (M1) keV transitions were found to agree with the measurements of Johns et al. However, the 234-keV transition, formerly thought to be an E2, is an M1 (< 9% E2 admixture). The multipolarities of the 717 and 875-keV lines agree with the

$\pi\sqrt{2}$ Internal Conversion Spectra

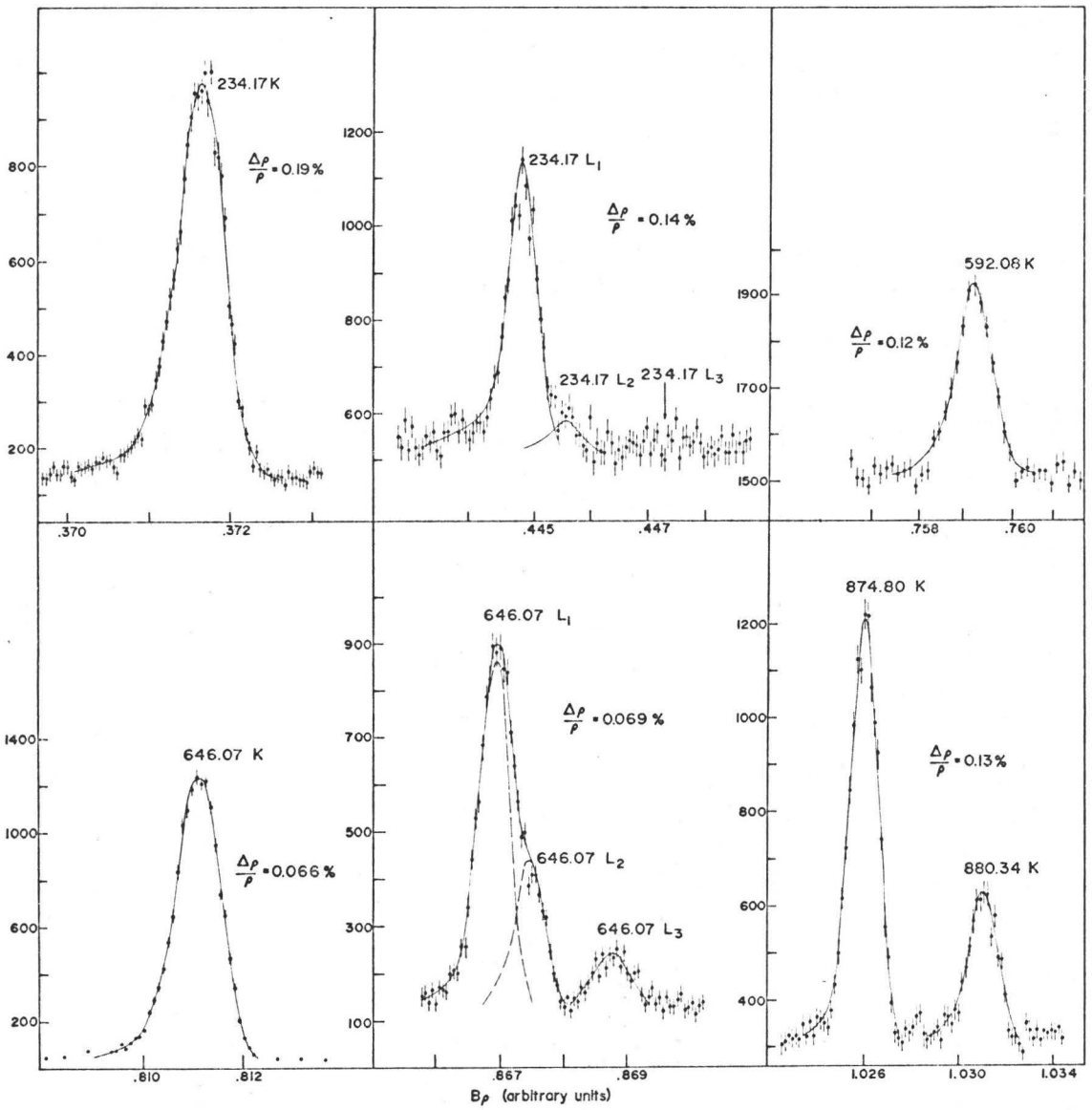

Figure 6

$\pi\sqrt{2}$ Internal Conversion Spectra

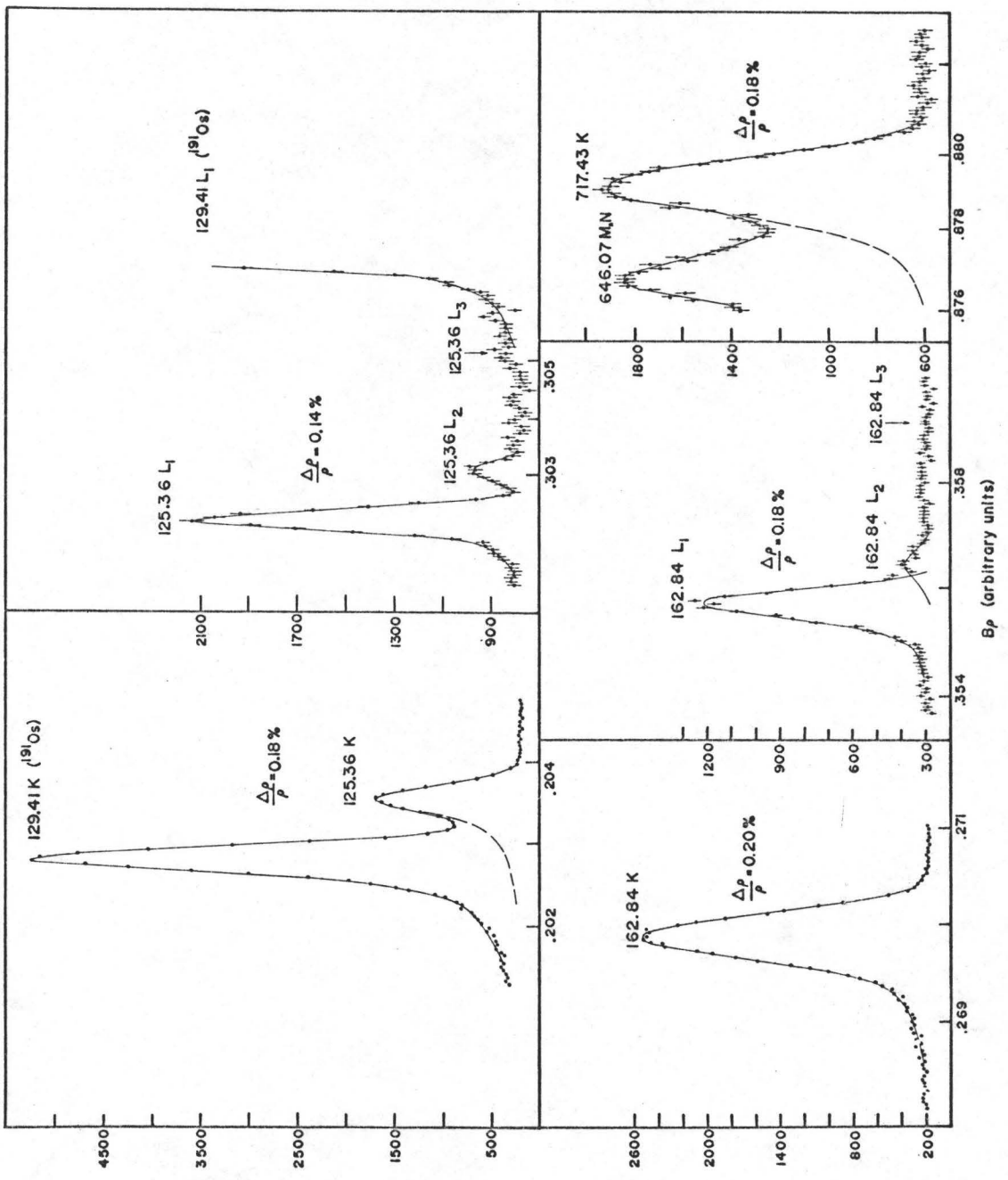

Figure 7

TABLE II

Conversion coefficients, multipolarities and intensities for transitions in ^{185}Re

Transition energy (keV)	Shell	Electron Intensities (per 100 decays) $\times 10^{+2}$	Conversion coefficients: Theoretical values M1	Conversion coefficients: Theoretical values E2	Conversion coefficients: Experimental	Assignment	Transition Intensities (%)
71.37±0.08	L_1	19.2 ±5.4	1.7	1.9×10^{-1}	$\frac{L_1}{L_2} > 4.9$		
	L_2	<2.8	1.65×10^{-1}	6.2			0.38
	L_3	<1.4	1.9×10^{-2}	6.0	$\frac{L_1}{L_3} > 9.9$		
	M_1	4.0 ±1.4	3.9×10^{-1}	5.2×10^{-2}		M1	
	M_2	<1.2	4.1×10^{-2}	1.5	$\frac{M_1}{M_2} > 2.2$	(<2.5%E2)	
	M_3	<0.54	4.6×10^{-3}	1.5	$\frac{M_1}{M_3} > 4.8$		
125.36±0.04	K	80.6 ±4.5	2.25	5.35×10^{-1}	2.10±0.15		
	L_1	19.0 ±0.77	3.45×10^{-1}	5.9×10^{-2}			
	L_2	2.1 ±0.21	3.25×10^{-3}	5.1×10^{-1}	$\frac{L_1}{L_2} = \pm^{9.1}_{0.8}$	M1 (<1.5%E2)	1.5
	L_3	<1.3	3.55×10^{-3}	4.2×10^{-1}	$\frac{L_1}{L_3} > 14$		
157	K	<0.027	1.15	3.1×10^{-1}			
162.84±0.02	K	60.2 ±3.3	1.10	2.9×10^{-1}	0.84±0.15		
	L_1	9.6 ±0.4	1.6×10^{-1}	3.25×10^{-2}			
	L_2	0.84±0.23	1.5×10^{-2}	1.4×10^{-1}	$\frac{L_1}{L_2} = \pm^{11.5}_{3.2}$	M1 (<2.9%E2)	1.6
	L_3	<0.26	1.65×10^{-3}	1.05×10^{-1}	$\frac{L_1}{L_3} > 35$		

TABLE II (continued)

Conversion coefficients, multipolarities and intensities for transitions in ^{185}Re

Transition energy (keV)	Shell	Electron Intensities (per 100 decays) x 10^{+2}	Conversion coefficients: Theoretical values M1	Conversion coefficients: Theoretical values E2	Conversion coefficients: Experimental	Assignment	Transition Intensities (%)
229	K	<0.027	4.5×10^{-1}	1.2×10^{-1}			
234.17±0.02	K	16.8 ±0.6	4.2×10^{-1}	1.1×10^{-1}	0.39±0.06		
	L_1	2.5 ±0.18	5.85×10^{-2}	1.4×10^{-3}	$\frac{L_1}{L_2} = 11.8 \pm 4.2$	M1 (<9%E2)	0.66
	L_2	0.22±0.08	5.5×10^{-3}	2.95×10^{-2}			
	L_3	<0.11	5.75×10^{-4}	1.85×10^{-2}	$\frac{L_1+L_2}{L_3} > 23$		
592.08±0.05	K	1.45±0.12	3.35×10^{-2}	1.10×10^{-2}	(1.2±0.14) x 10^{-3}	E2 (<9%M1)	1.2
646.07±0.03	K	76.8	2.7×10^{-2}	9.45×10^{-3}	9.45×10^{-3} b)		
	L_1	10.8 ±1.1	3.95×10^{-3}	1.3×10^{-3}	$\frac{L_1}{L_2} = 2.6 \pm 0.3$	E2 (<3%M1)	82.2
	L_2	4.0 ±0.28	3.55×10^{-3}	5.6×10^{-4}			
	L_3	1.7 ±0.017	3.20×10^{-5}	1.95×10^{-4}	$\frac{L_1}{L_3} = 6.6 \pm 0.66$		
					$\frac{L_1+L_2}{L_3} = 9.2 \pm 0.7$		
717.43±0.08	K	4.3 ±0.35	2.0×10^{-2}	7.65×10^{-3}	(1.07±0.12) x 10^{-2}	(75±12) E2	4.0

TABLE II (continued)

Conversion coefficients, multipolarities and intensities for transitions in ^{185}Re

Transition Energy (keV)	Shell	Electron Intensities (per 100 decays) x 10^{+2}	Conversion coefficients			Assignment	Transition Intensities (%)
			Theoretical values		Experimental		
			M1	E2			
874.80±0.07	K	7.8 ±0.45	1.2 x 10^{-2}	5.1 x 10^{-3}	(1.13±0.12) x 10^{-2}	($93^{+}_{-}15$) % M1	7.0
880.34±0.10	K	3.0 ±0.3	1.2 x 10^{-2}	5.05x 10^{-3}	(5.37±0.82) x 10^{-3}	E2 (<16% M1)	5.6
930.8	ΣL	(0.98±0.39) x 10^{-2} c)	1.7 x 10^{-3}	7.8 x 10^{-4}	(2.0±0.9) x 10^{-3}	M1 (<65%E2)	0.05

a) Normalized to 646 K

b) Normalized value, assuming that the E2 character of this transition, as seen from the L subshell ratios is valid.

c) Measurements from Si(Li) detector.

results of Metzger, who inferred from his results that the 717 had to be predominantly E2 and that the 875 had to be predominantly M1. The 880-keV line is E2 (< 16% M1); unfortunately, Metzger was unable to excite this level in his work so that no comparison can be made. Upper limits of 0.027×10^{-2} were set on the intensity of the 158 and 229 K-conversion lines. If it is assumed that these transitions are pure M1, then upper limits of 2×10^{-4} and 6×10^{-4} were set on the γ-intensities (per 100 decays) of these transitions; these limits were about a factor of 100 lower than the limits set by the γ-measurements.

6.3 Silicon Detector Measurements

In addition to the $\pi\sqrt{2}$ measurements, an internal conversion spectrum was taken on the silicon detector described in Chapter V. The spectrum is shown in Figure 8. From this measurement, the α_L of the 931-keV transition to the 5/2+ ground state was found to be $(2.0 \pm 0.9) \times 10^{-3}$. Although the error is large, a pure E2 is not allowed; the transition appears to be M1, but the errors would allow up to a 65% E2 admixture. This conversion coefficient implies a spin and parity of 3/2+, 5/2+, or 7/2+ for the 931-keV level. The 7/2 choice is ruled out by the fact that the level is fed by electron capture from the 1/2- ground state of ^{185}Os.

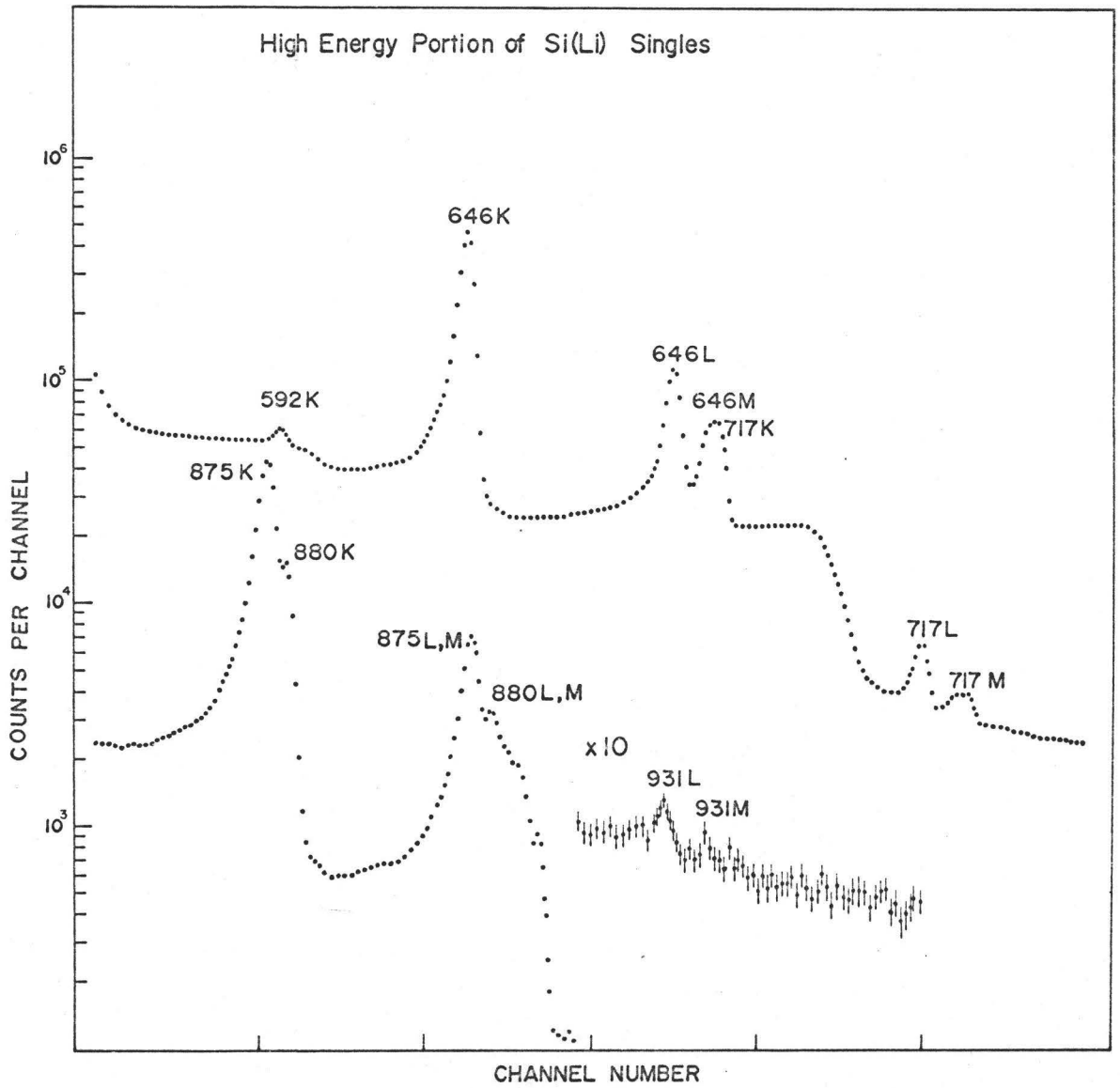
High Energy Portion of Si(Li) Singles
COUNTS PER CHANNEL
CHANNEL NUMBER
646K
646L
646M
592K
717K
875K
880K
875L,M
880L,M
717L
717 M
x10
931L
931M

Figure 8

6.4 KLX and KXY Auger Spectra

An attempt to remeasure the L-conversion lines of the 71-keV transition between the 717 and 646-keV levels was complicated by the presence of the KLX Auger spectrum in the same region. Initially, there was some doubt as to whether the conversion lines actually exist. In view of this, it was also decided to scan the region which contained the 71-M conversion lines; here the presence of the KXY Auger group was a complicating factor. By combining these two measurements, it was hoped that the existence of the 71-keV transition could be proved and that its multipolarity could be measured.

Figure 9 shows the region of the KLX Auger spectrum with the expected positions of the L-conversion lines and the positions of all the Auger transitions indicated. Below the spectrum are shown the intensities of the Auger lines measured for ^{183}Re by Newton (1960). These measurements were taken with a permanent magnet type of 180° spectrograph with photographic recording. The Auger intensities, measured for the neighbouring nucleus ^{169}Tm by Gizon (1968) with a double-focussing 50-cm radius β-spectrometer with a resolution of 0.1%, are shown below the ^{183}Re intensities for comparison. The resolution in this latter work was comparable to that used in the present work.

Table III shows a comparison of the energies of the Auger transitions in ^{183}Re with those found for ^{185}Re in the

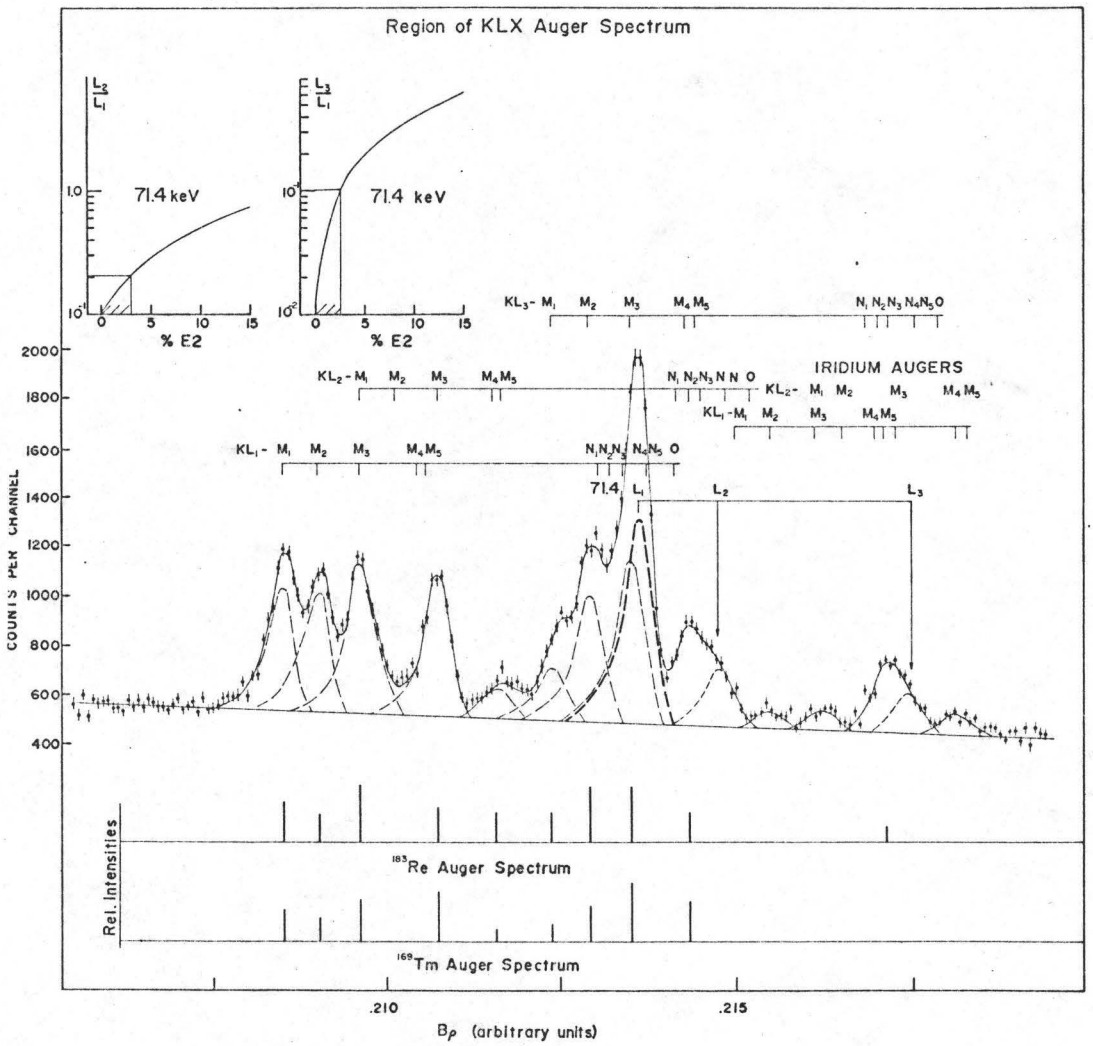
Region of KLX Auger Spectrum
71.4 keV
% E2
71.4 keV
% E2
IRIDIUM AUGERS
COUNTS PER CHANNEL
Rel. Intensities
183Re Auger Spectrum
169Tm Auger Spectrum
Bρ (arbitrary units)

Figure 9

TABLE III

Auger Transitions for ^{185}Re and Neighbouring Nuclei

Auger Transitions	Present Work		^{183}Re b)		Intensity a)				
	Energy	Intensity a)	Energy	Intensity a)	^{169}Tm c)	^{175}Lu d)	^{183}W e)	^{203}Tl f)	^{207}Bi g)
KL_1M_1	56.14±0.05	100	56.19	100	100	100	100	100	100
L_1M_2	56.39±0.05	124±33	56.39	68	77	78	87	81	125
L_1M_3, L_2M_1	56.71±0.05	155±36	56.68	141	136	130	100	127	213
L_2M_2			56.91						L_2M_2
$L_1M_4M_5$, L_2M_3	57.28±0.05	140±30	57.30	86	162	112	58	77	213
L_2M_4,M_5	57.75±0.05	40±10	57.71	73	41	23	...	25	244
L_3M_1	58.13±0.06	55±16	58.11	73	54	35	83	119	44
L_3M_2	58.40±0.06	130±50	58.35	134	113	105	117		112
L_3M_3	58.70±0.06	170±70	58.65	136	128 N_1	138 N_1	150	81	
L_1N					62 N_2,N_3	13 N_2,N_3			530

(continued next page)

TABLE III (continued)

Auger Transitions for ^{185}Re and Neighbouring Nuclei

Auger Transitions	Present Work		^{183}Re b)		Intensity a)				
	Energy	Intensity a)	Energy	Intensity a)	^{169}Tm c)	^{175}Lu d)	^{183}W e)	^{203}Tl f)	^{212}Bi g)
L_3M_4,M_5					L_1N_4,N_5	L_1N_4,N_5			
L_1O					77	53			
L_2N	59.13±0.08	87±47	59.15	73			83	66	
					N_2,N_3,O	N_2,N_3,O			
L_2O					51	30			
L_3N	60.62±0.08	32±16	60.66	36	...	...	33	56	88
L_3O			61.08						
KMM		160±35						65	
KMN		74±40						29	320
KNN		...						10	

a) Normalized to 100 for KL_1M_1

b) Newton (1960)

c) Gizon (1968)

d) Gizon et al (1967)

e) Gallagher et al (1958)

f) Sujkowski (1961)

g) Mladjenović et al (1955)

present investigation. The table also makes a comparison of the Auger transitions which have been measured for some heavy nuclei (Tm, Lu, W, Re, Bi and Hg) with those obtained in this work. The various sets are normalized to a value of 100 for the KL_1M_1 transition.

The ^{185}Os shows a large peak at an energy corresponding to the L_1 conversion of a 71.4-keV gamma ray. The observed peak includes the fairly strong KL_3M_3 Auger line at an energy of 58.70 keV. The presence of this peak increases the uncertainty in the conversion line intensity and the limits of error given reflect this fact. If the observed peak were predominantly due to the KL_3M_3 Auger, its position would have been shifted by ~ 0.5 of a line width toward lower energies. It is thus clear that the data cannot be explained by the Auger contribution alone. The problem is further complicated by the presence of the weaker KLNO Auger lines which are directly under the 71.4 L_1 peak. While these have not been individually resolved in any of the Auger spectra, they appear to be ~ 20% of the intensity of the KL_1M lines. This fraction was used in estimating the intensity of the L_1 conversion line.

The much weaker L_2 conversion is obscured by the KL_2NO Auger group and the L_3 line by the KL_3NO and the KLM Auger groups from Iridium associated with the ^{191}Os impurity. Because of these Augers, it has been only possible to set rather high upper limits on the L_2 and L_3 conversion line

intensities. From these upper limits and from the lowest possible value for the intensity of the L_1 line, the lower limits for the L subshell ratios, tabulated in Table II, were obtained.

The region spanning the KXY Auger groups is shown in Figure 10. The expected positions of the M-conversion lines of the 71.4-keV transition and the positions of the KMM and KMN Auger lines are shown. An analysis similar to that performed above for the L-conversion lines was made to try to separate the 71-M conversion lines from the complex Auger spectrum. The M1 line is clearly evident and upper limits have been set on the existence of the M_2 and M_3 conversion lines. Using this data, lower limits for the M subshell ratios have been determined.

Using the experimental subshell ratios and the graphs of subshell ratio vs % E2 mixing shown in Figures 9 and 10, upper limits for the E2 admixture in the 71-keV transition were found. From these values ($\frac{L_2}{L_1} < 3\%$, $\frac{L_3}{L_1} < 2.5\%$, $\frac{M_2}{M_1} < 9\%$), $\frac{M_3}{M_1} < 5\%$), the multipolarity of the 71-keV transition was found to be M1 (< 2.5% E2). The theoretical conversion coefficients were taken from the tables of Hager and Seltzer (1968). From the intensity (relative to the 646-keV line) of the L_1 conversion line and from the multipolarity, the intensity of the γ-transition has been established at 0.11 ± 0.03 (per 100 decays). Such a gamma ray would have been masked by the K_β X-rays in the direct spectrum.

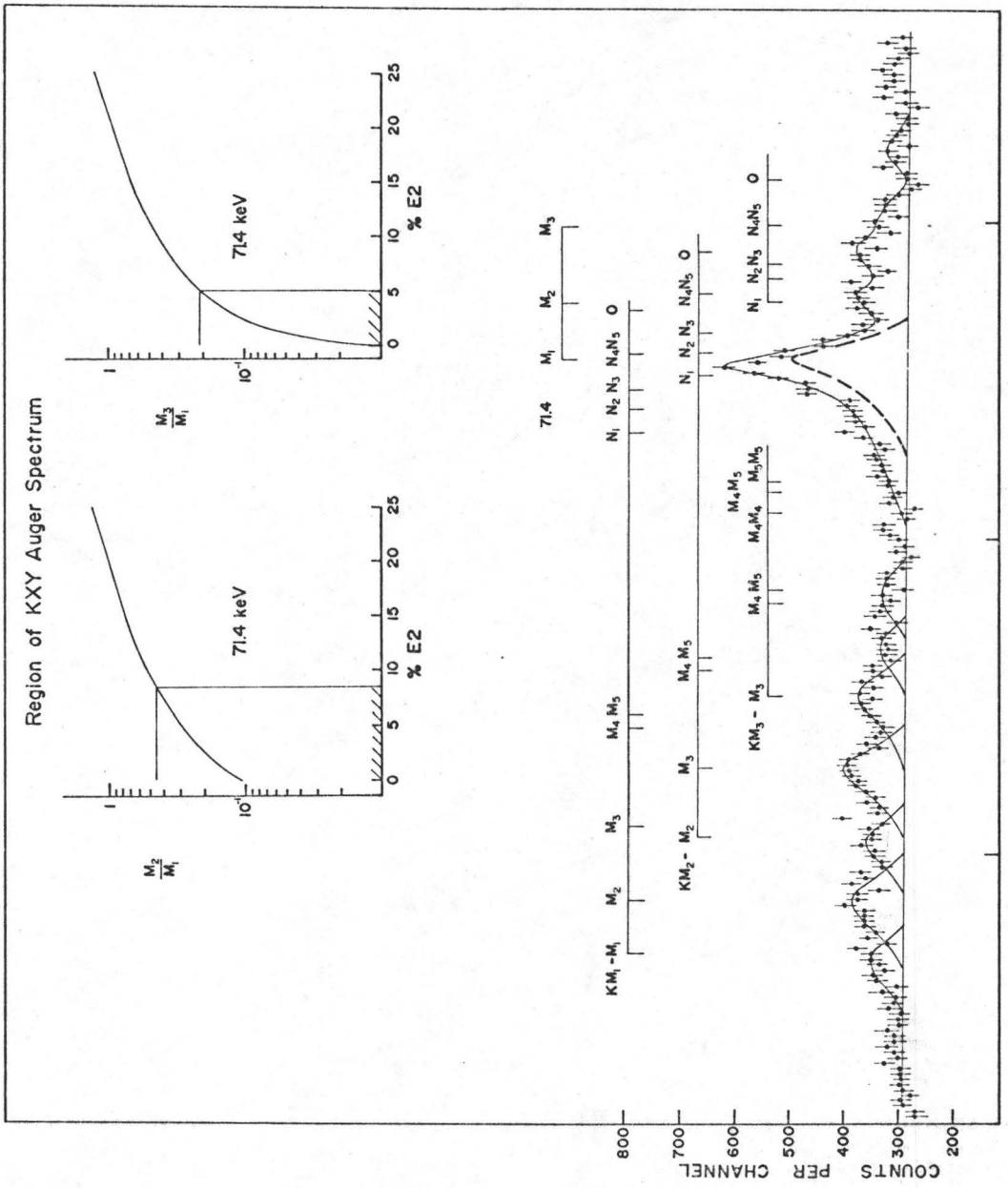
Region of KXY Auger Spectrum
M2/M1
71.4 keV
% E2
M3/M1
71.4 keV
% E2
71.4
KM1 - M1
KM2 - M2
KM3 - M3
COUNTS PER CHANNEL
Bρ (arbitrary units)

Figure 10

6.5 Gamma-Gamma Coincidence Results

The coincidence data was sorted into matrix form in the manner described in Chapter III. Projections onto both axes were plotted and are presented in Figure 11; these represent the summed projections from two data tapes. Coincidence spectra resulted from the summing of spectra in coincidence with several adjacent channels along either axis. In this way, "gates" at any energy and of any width could be chosen. Background was subtracted if necessary; that is, spectra in coincidence with channels adjacent to the peak are summed and then subtracted from the spectra in coincidence with the channels constituting the peak. The "difference spectra" so obtained are a good approximation to the spectrum in coincidence with a single γ-ray. One can plot either the Ge(Li) "difference spectra" in coincidence with NaI gates or the NaI "difference spectra" in coincidence with Ge gates. However, it is difficult in the first choice to determine the correct background to be subtracted and so it was found more useful to concentrate on the NaI coincidence spectra associated with photopeaks in the Ge(Li) detector from individual gamma rays. These spectra are presented in Figure 12 and the coincidence probabilities deduced from these spectra are given in Table IV.

All the spectra show the expected strong X-ray peaks. In addition the NaI spectrum in coincidence with the 125-keV gamma ray reveals peaks at 592 and 163-keV. The 129-keV peak

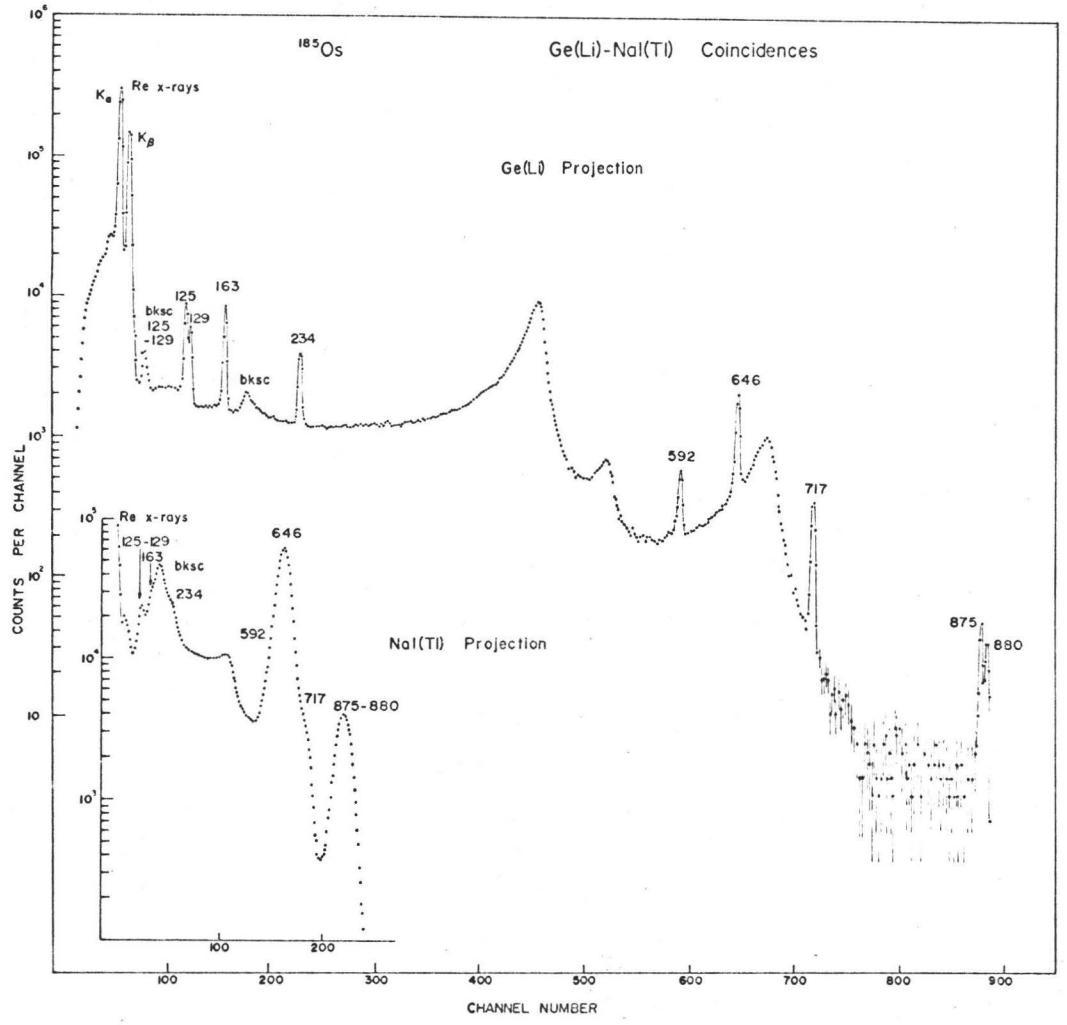
^{185}Os
Ge(Li)-NaI(Tl) Coincidences
Ge(Li) Projection
NaI(Tl) Projection
Re x-rays
K_α
K_β
125
129
bksc
125
-129
163
234
bksc
592
646
717
875
880
875-880
COUNTS PER CHANNEL
CHANNEL NUMBER

Figure 11

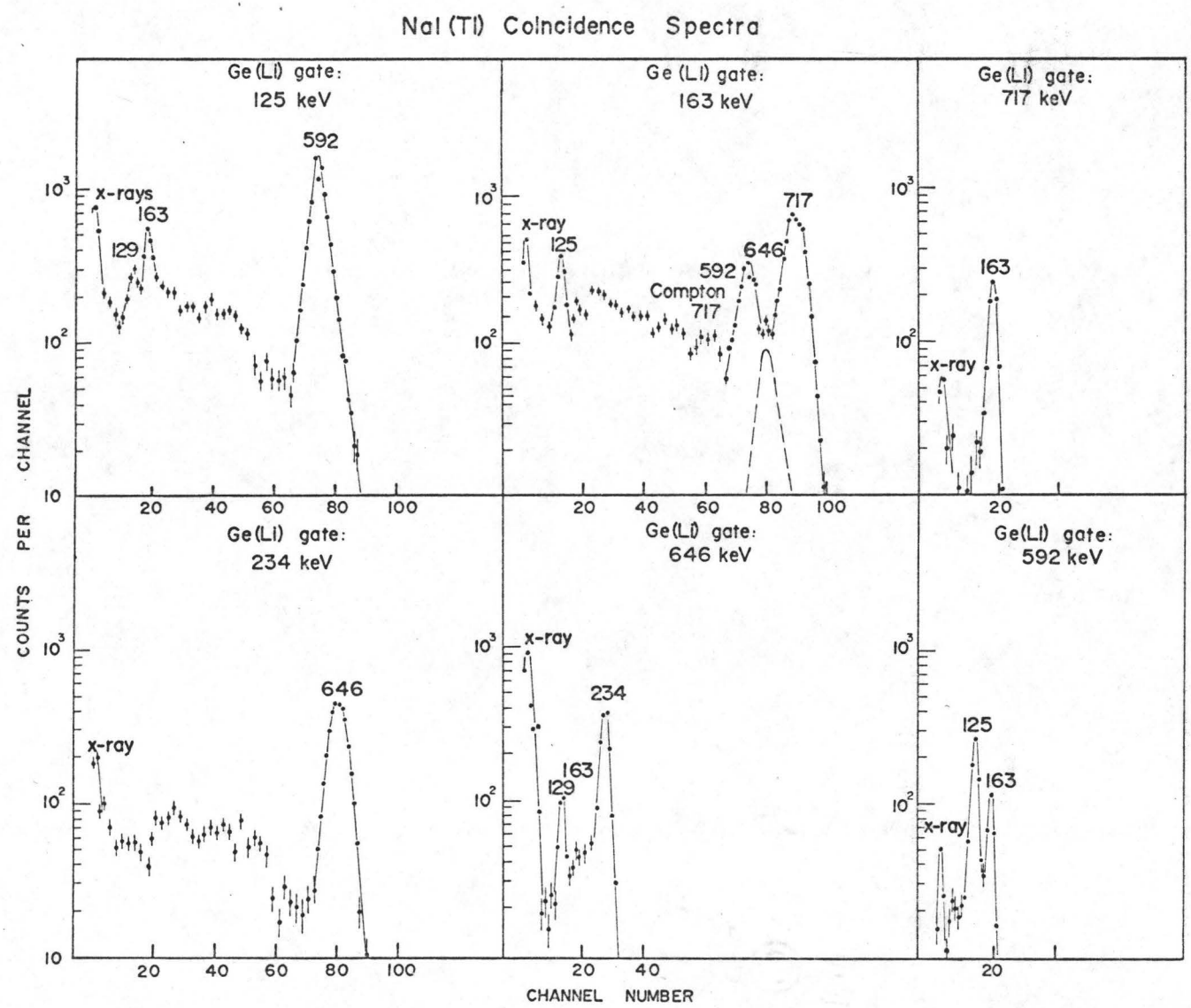
NaI (Tl) Coincidence Spectra
Ge(Li) gate:
125 keV
592
x-rays
163
129
Ge (Li) gate:
163 keV
717
x-ray
125
592
646
Compton
717
Ge(Li) gate:
717 keV
163
x-ray
Ge(Li) gate:
234 keV
646
x-ray
Ge(Li) gate:
646 keV
x-ray
234
163
129
Ge(Li) gate:
592 keV
125
163
x-ray
COUNTS PER CHANNEL
CHANNEL NUMBER

Figure 12

is due to chance events associated with the strong ^{191}Os line at this energy. The 163-keV gate reveals peaks at 125, 592 and 717-keV with a weak peak at 646-keV. Similarly,the 234-keV gate shows a strong 646-keV peak, the 646-keV gate shows a 234-keV peak along with a weak 163-keV peak; the 717-keV gate brings up a 163-keV peak and the 592-keV gate, peaks at 125 and 163-keV.

The number of coincidences between γ_i and γ_j is given by

$$N_{ij} = N_o(\varepsilon\omega)_i(\varepsilon\omega)_j C_{ij}$$

where C_{ij} is the probability of γ_i being in coincidence with γ_j. The values of $(\varepsilon\omega)$ for the Ge(Li) detector were derived from the singles spectrum taken during the experiment, using the photon intensities of Table I. This automatically corrected for geometrical effects on the Ge(Li) side. The $(\varepsilon\omega)$ values for the NaI(Tl) detector were taken by combining Heath's efficiency tables (1964) with the absorption factors relevant to the 1.8 mm of cadmium covering the NaI(Tl) detector. The value of N_o was obtained by using the 234-646 coincidence rate which, according to the decay scheme, has a C_{ij} value of 0.45%. The first two columns of Table IV show the pair of gamma rays involved; the next two columns give the C_{ij} and C_{ji} values appropriate to this pair. In this nomenclature, the first suffix refers to the gamma ray detected in the Ge(Li) detector

TABLE IV

Coincidence Probabilities from Ge(Li)-NaI(Tl) Experiments

		Experimental C_{ij}			Expected from Decay
E_i	E_j	C_{ij}	C_{ji}	Avg.	C_{ij}
125	163	0.037	0.034	0.036	0.05
	592	0.46	0.38	0.42	0.40
163	592	0.16	0.16	0.16	0.15
	646	0.051	0.055	0.053	0.049
	717	0.39	0.38	0.39	0.51
234	646	0.45	0.45	0.45*	0.45*

*normalized value

and the second to the gamma ray observed in the NaI(Tl) detector. Since the system is symmetric these two values should agree. The fifth column presents the average C_{ij} values while the last gives the C_{ij} expected from the decay scheme. The agreement between the experimental and predicted values is quite gratifying and confirm the correctness of the decay scheme.

The existence of 163-646 coincidences implies the presence of a 71.4-keV gamma ray which is strongly converted and masked by the X-rays in the γ-γ coincidence experiments. The measured C_{ij} for this pair of gamma rays can be used to deduce the intensity of this transition using the relation

$$C_{646-163} = \frac{I_{163} \times T_{71.4}}{(T_{717}+T_{592}+T_{71.4})}$$

In this relation I refers to photon intensities and T to transition intensities. This relationship yields an intensity of $0.45 \pm 0.10\%$ for the 71.4-keV transition. This value is consistent with the M1 character of this as revealed by the internal conversion data; the photon part of this intensity is approximately 0.15% with the balance arising from internal conversion.

6.6 Measurement of the Decay Energy

Figure 13 presents the results of the two and a half week K X-ray-gamma ray coincidence experiment discussed in Chapter V. The Ge projection reveals a definite peak at 930.9

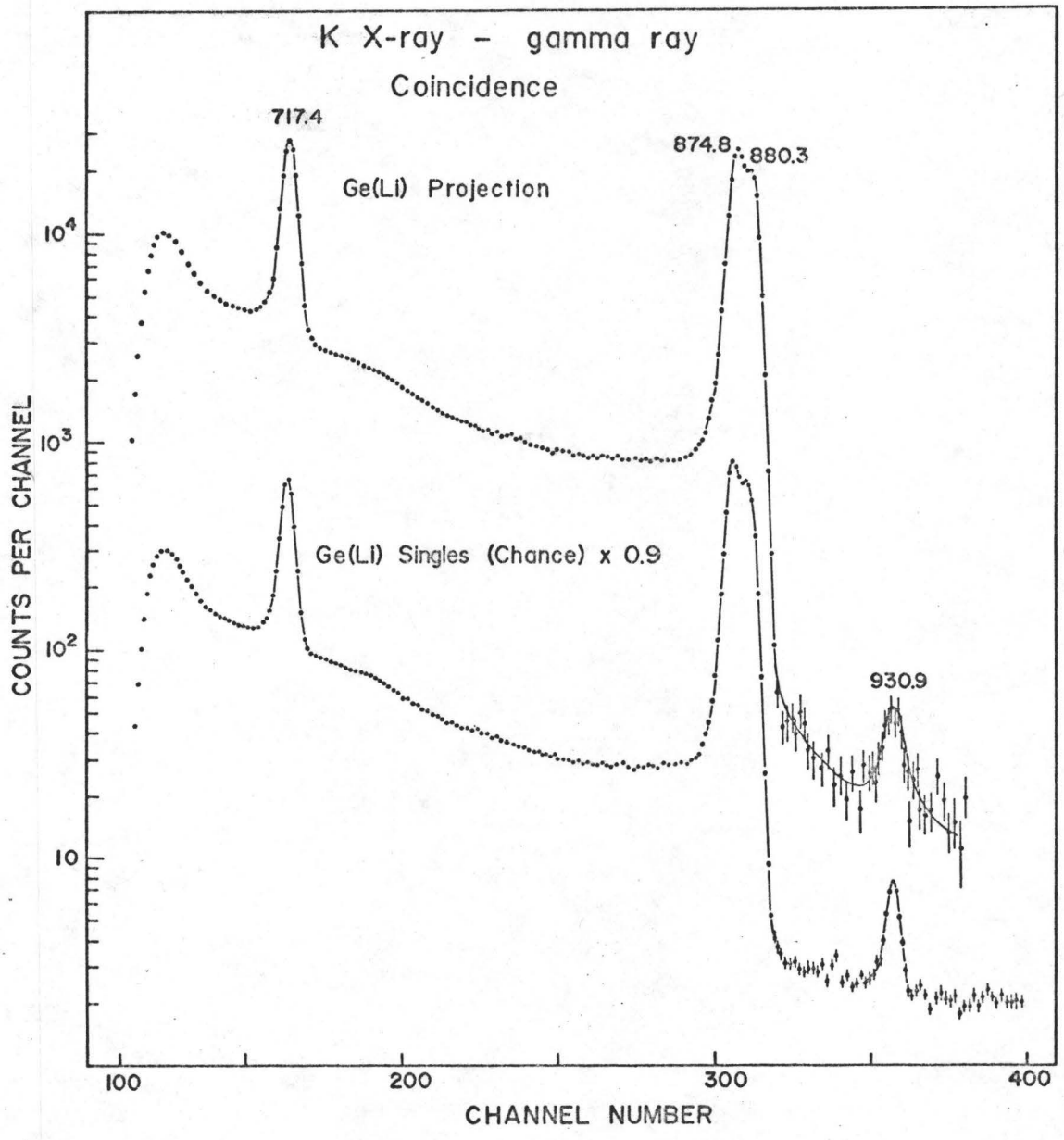
K X-ray - gamma ray
Coincidence
717.4
874.8
880.3
Ge(Li) Projection
Ge(Li) Singles (Chance) x 0.9
930.9
COUNTS PER CHANNEL
10⁴
10³
10²
10
100
200
300
400
CHANNEL NUMBER

Figure 13

keV. Inasmuch as the total number of true coincidences and the total number of chance counts were recorded during the experiment, the true/chance ratio was well defined as 36:1. Since the chance spectrum has the same shape as the singles spectrum, this ratio could then be applied to a singles spectrum recorded during part of the run to obtain the actual chance spectrum, as presented in Figure 13. It is clear from the figure that the chance contribution to the 931-keV peak is 10% of the total. It is also clear that the 931 peak is much less intense relative to the 717-keV peak in the coincidence spectra than it is in the singles (see chance spectrum). This indicates that most of the transitions to the 931-keV level is due to L or higher shell capture. The presence of a large amount of L-capture to the 880-keV doublet can also be seen by comparing the ratio of intensities of the 717 and 875-880 keV peaks in the coincidence and singles spectra.

Using the relation developed in Chapter II, an analysis of the data gave the following results:

$$\frac{P_K(875\text{-}880)}{P_K(646)} = 0.715 \pm 0.050 \qquad \frac{P_K(931)}{P_K(875\text{-}880)} = 0.145 \pm 0.064$$

These ratios were determined in different experiments; the $P_K(931)/P_K(646)$ ratio could not be determined in the 2-1/2 week run because the discriminators were set to eliminate the 646-keV peak. For the analysis, the 875 and 880 levels were considered together, the energy taken being an average value. One advantage

of this method is that the result is independent of the existence of a transition from the 880 to the 875-keV level (such a transition was proposed by Schulz (1967)). The measured K X-ray-646-keV coincidence rate was corrected for the contributions of X-rays from the K-conversion of the 163 and 234-keV transitions and for the X-rays from K-capture to the 717 and 880-keV levels. This total correction amounted to 0.6%.

Theoretical curves calculated from the equation given in Chapter II are shown in Figure 14. The curves give a ratio of P_K's to different levels (P_K being defined as the probability of K-capture to the total capture probability). The preliminary experiment, which did not involve the 931-keV transition, gave a value of 1011^{+11}_{-8} keV for the decay energy. In fact it was this value, which indicated that K-capture could occur to the 931 level, that led to the second experiment to look for K X-ray coincidences with the 931-keV γ-ray. This second experiment gave a value of 1012 ± 2.5 keV for the decay energy. The two values agree very well. Both agree with the value of 1010 ± 4 keV obtained by Schulz. The fact that K X-ray coincidences do occur with the 931 proves beyond doubt that the 931-keV transition belongs to the ^{185}Os decay.

This value of the decay energy is in serious disagreement with the earlier measurements obtained in this laboratory

Figure 14

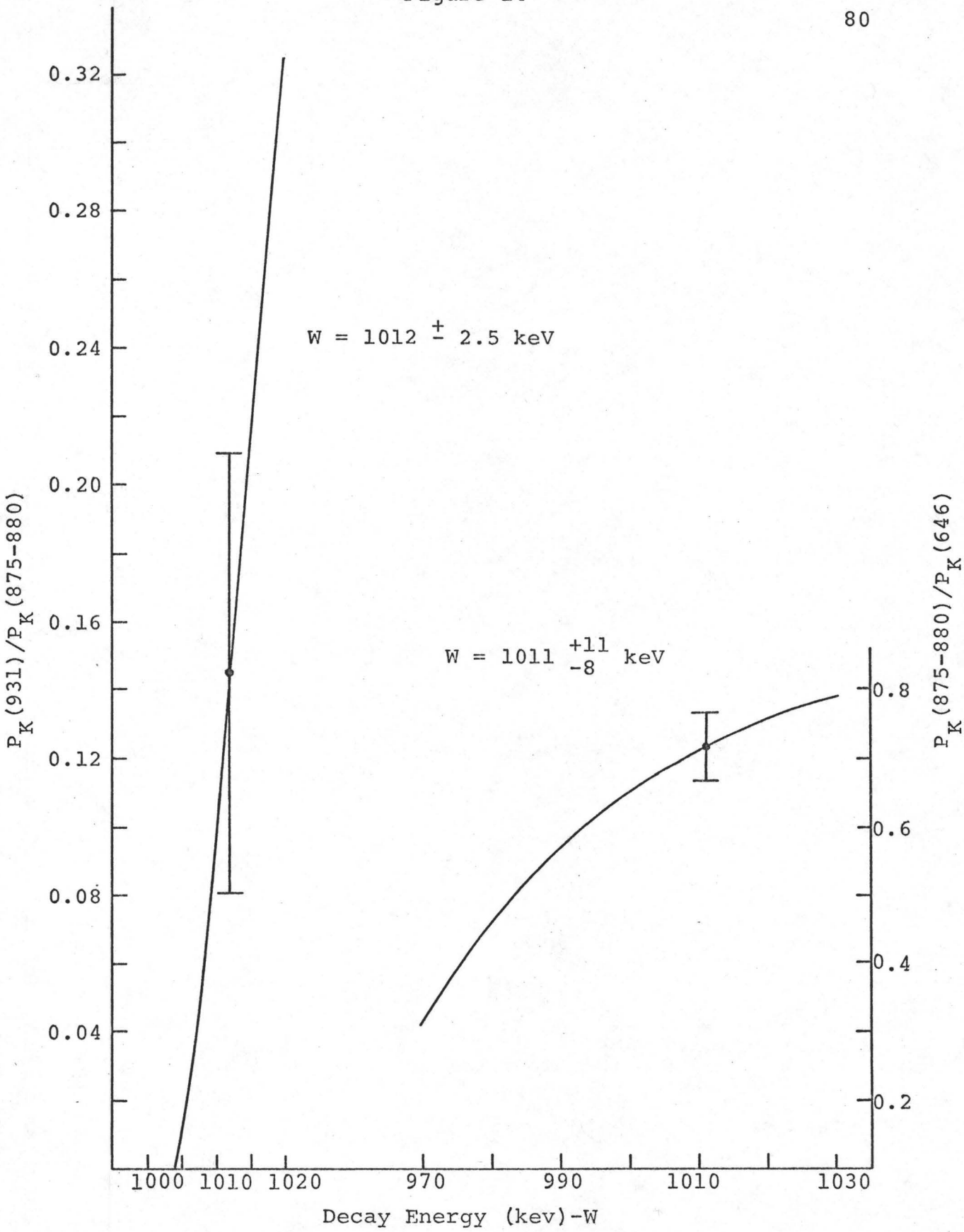
0.32
0.28
0.24
0.20
0.16
0.12
0.08
0.04
$P_K(931)/P_K(875\text{-}880)$
W = 1012 ± 2.5 keV
W = 1011 $^{+11}_{-8}$ keV
0.8
0.6
0.4
0.2
$P_K(875\text{-}880)/P_K(646)$
1000 1010 1020
970 990 1010 1030
Decay Energy (kev)-W

(Johns et al 1957). The disagreement is mainly due to revisions in the theory since that date which predict a significant increase in the probability of M and higher shell capture. There are slight revisions in the energies of the gamma rays involved. When the new theory and the new energies are used with their measured values, their decay energy increases from 985 $\pm$ 7 keV to 1001 $\pm$ 7 keV which is almost consistent with the present value.

6.7 The Decay Scheme

The decay scheme resulting from the present investigation is shown in Fig. 15 . It differs only slightly from the decay scheme first proposed by Johns et al (1957) and subsequently confirmed by other workers. The additions to the scheme from the present work are (1) the inclusion of the 931-keV level and (2) clear proof that the spin of the 880-keV is 1/2+. Subsequently, each of the levels will be discussed in turn.

The information concerning the decay energy, the capture ratios (P_K) and the transition intensities makes it possible to calculate the log $f_o t$ values for the electron capture transitions to each state, using the expression

$$f_o t = \frac{\pi}{2} G_K^2 (Q-B_K)^2 t_K$$

In this expression $\frac{\pi}{2} G_K^2 = 4.148$ (see tables by Zyryanova (1963), the expression $(Q-B_K)$ is evaluated in $m_o c^2$ units, and t_K is the partial half-life for K-capture. Similarly one can obtain $f_o t$

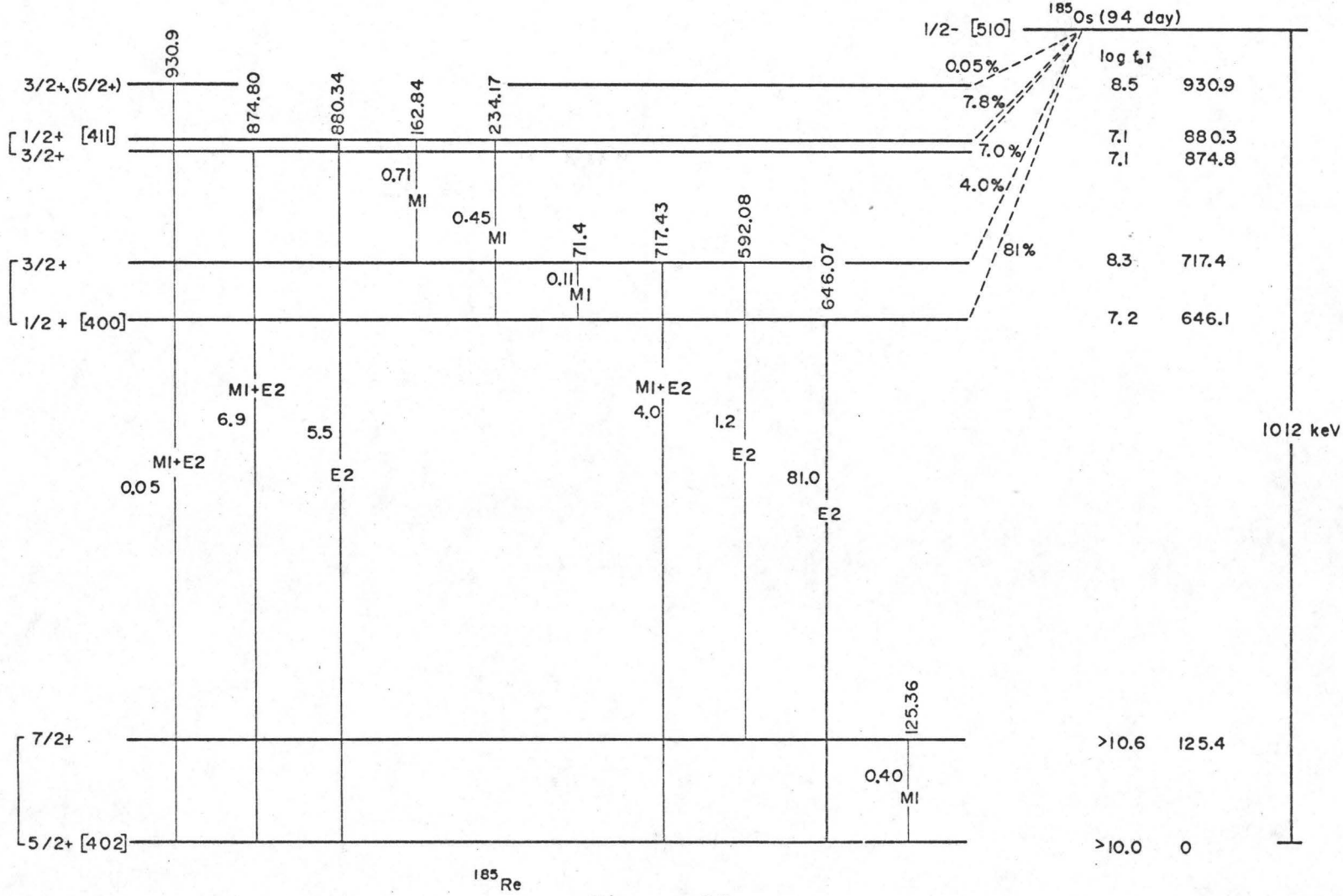

Figure 15

The Decay Scheme of ^{185}Os

from the L-capture intensities using the relation $f_o t = \frac{\pi}{2} G_{L_1}^2 (Q-B_{L_1})^2 t_{L_1}$ where $\frac{\pi}{2} G_{L_1}^2 = 0.603$. The values of $f_o t$ derived from the two formulae are in good agreement and only the values derived from K-capture will be presented in the table below.

Level fed (keV)	Electron capture intensity (%)	P_K	log $f_o t$
0	<1.0		>10
125	<0.2		>10.6
646	81	0.77	7.2
717	4	0.75	8.3
875	7	0.56	7.1
880	7.8	0.55	7.1
931	0.05	0.08	8.5
(768)	<0.006	0.72 (est)	>11
(836)	<0.006	0.6 (est)	>10.6

The lower limits on log $f_o t$ set for the ground state is based on the assumption that not more than 1% of the transitions proceed to this level. The 768 and 836-keV levels, seen in inelastic scattering experiments, are included in the table since their spin assignments are suggestive of possible electron capture to these levels.

The ground state of ^{185}Re, which was measured to be 5/2+ (Lindgren 1965), was assigned to the 5/2+[402] Nilsson orbital (Mottelson and Nilsson 1959). The value of the magnetic moment measured by nuclear magnetic resonance, is in agreement with that predicted for the Nilsson 5/2+[402] orbital. The ground state of ^{185}Os was assigned to the 1/2-[510] configuration.

The 125.4-keV level is well-established as the 7/2+ member of the rotational band built on the 5/2+ ground state. This level and the 9/2+ member at 285-keV have been populated by the Coulomb excitation experiments of many workers (e.g. McGowan and Stelson 1958 and de Boer et al 1959). Recently, in the inelastic scattering experiments of Bisgård and Veje (1967), the 11/2+ and 13/2+ members were found. The 125.36-keV M1 transition to the ground state and the absence of electron capture feeding to this level is consistent with a 7/2+ assignment.

The 646.1-keV level is a 1/2+ state. The level is strongly populated from the ^{185}Os decay; it decays to the 5/2+ ground state with a pure E2 transition, but there is no transition to the 125-keV level. The accepted spin assignment of 1/2 makes the latter transition an M3 which is not expected to compete with the strong E2 ground-state transition; if the spin were 3/2, the E2 transition to the 7/2+ rotational state built on the ground state should be of comparable strength (Alaga et al 1955) .

The 646-keV level was interpreted by Mottelson and Nilsson as a 1/2+[400] orbital. Gallagher et al (1960), in a study of ^{187}Re, indicated that a γ-vibrational description of some of the states, rather than an intrinsic one, might be more reasonable. The 646-keV level would then be the K-2 vibrational state built on the 5/2+[402] ground state and would correspond to the 511.6-keV level in ^{187}Re. The microscopic treatments of odd-mass gamma vibrations by Bès and Cho (1966) and by Soloviev and Vogel (1967) predict a large admixture of the 1/2+[400] one-quasiparticle state and a predominant 5/2+[402]p,{3/2-[512],1/2-[510]}n three-quasiparticle component in the structure of the lowest K=1/2+ state of ^{185}Re.

The 717.4-keV level is directly populated in the ^{185}Os decay. It decays by an M1+E2 transition to the 5/2+ ground state, by an E2 transition to the 7/2+ level at 125 keV and by an M1 transition to the 1/2+ state at 646 keV. Its spin is therefore uniquely determined as 3/2+. This choice is consistent with Metzger's conclusions that a 1/2+ spin is improbable; the B(E2↓)'s for the 717, 646 and 592-keV transitions are of comparable magnitudes as expected for γ-radiation connecting two rotational bands. These measurements are consistent with the assignment of this level as the 3/2 member of the rotational band built on the 646 keV level. The inelastic scattering experiments of Bisgård and Veje populated the 1/2, 3/2 and 5/2 members of this band with levels at 646, 717 and

768 keV; a similar band is found in ^{187}Re. Furthermore, Bisgård et al (1965) found evidence for the 3/2+ member of this band in the β-decay of ^{187}W; however they were unable to find the 71-keV transition between the 582 and 511-keV levels due to the Auger lines (KLM and KLN) and the strong 72 L lines.

A comparison of the absolute experimental transition probabilities with the theoretical calculations (Faessler 1964) based on the two interpretations of the 646-keV band was made by Metzger (1967). Taking the theoretical results at face value, his experimental results favour the identification of the 646-keV state with the 1/2+[400] orbital. However, the results of Bisgård and Veje indicate a decoupling parameter larger than that calculated for a pure 1/2+[400] state. It would seem that the question of the character of this band is still open.

The 874.8 and 880.3-keV levels are directly populated in the decay of ^{185}Os. The 875 keV level de-excites only through a ground-state transition; no branching was found to the 646 and 717-keV levels. The present internal conversion measurement indicates that it is pure M1, although the errors allow up to 20% admixture of E2. This agrees with Metzger's conclusions that the transition is predominantly M1. The extent of the E2 hindrance may be deduced from the absence of a 749-keV transition (<0.007) to the 7/2 member of the ground state rotational band at 125 keV. The 880 keV level is de-excited by means of

M1 transitions to the 646 and 717 levels and by an E2 transition (< 16 % M1) to the ground state; there is no transition to the 125 level. The experimental results indicate spin assignments of 3/2+ and 1/2+ for the 875 and 880 levels. These levels were not populated in the inelastic scattering experiments of Bisgård and Veje. These levels have been assigned to the 1/2+[411] Nilsson orbital; this orbital is known to give rise to narrow doublets having large decoupling parameters (in the present case, the energy separation is 5.5 keV). The inversion of the band members is also found for the corresponding 618 and 625-keV levels in ^{187}Re (Bisgård et al 1967).

The 931-keV level, directly populated in the decay is de-excited by an M1 (or M1+E2) transition to the ground state. A spin of 3/2+ or 5/2+ can be assigned to this level. Two possible candidates for the 3/2+ choice are the 3/2+[411] and the 3/2+[402] Nilsson states; these are made on the basis of energy considerations. In the neighbouring nucleus ^{187}Re, the 3/2+[402] orbital is found at 773-keV, the 3/2+[411] at 865-keV; both are found above the 1/2+[411] orbital. The fact that the 3/2+[402] orbital is found at a lower energy in ^{187}Re would suggest that the 931-keV level corresponds to this orbital. However, the results of Bisgård and Veje indicate that the 836-keV level, populated in their inelastic scattering experiments, has a similar cross-section to the 773 3/2+[402] level in ^{187}Re. Electron capture to such

level would require a first-forbidden hindered transition. A lower limit of 10.6 was set on the log $f_o t$ of electron capture transitions to this level; such a value would be consistent with the above. The 3/2+[402] orbital was found below the 1/2+[411] orbital in ^{183}Re (Newton 1960), so it is possible that the 836-keV level could be the 3/2+[402]. If this is so, then the 931 level is probably the 3/2+[411] Nilsson state. A possible candidate for the 5/2+ choice is the 5/2+ member of the 1/2+[411] band which would be found at about this energy. The fact that the 5/2+ member of the band built on the 646 level is not populated in the decay (log $f_o t > 11$) would imply that the 5/2 member of the 1/2+[411] band would not be populated either. In view of this, the 3/2+ choice is favoured for the 931 level although the 5/2+ choice cannot be ruled out.

SUMMARY

The gamma ray transitions following the decay of 94-day ^{185}Os have been studied by singles and coincidence techniques using Ge(Li) and NaI(Tl) detectors. The internal conversion spectrum has been investigated using the Chalk River $\pi\sqrt{2}$ β-spectrometer and a Si(Li) detector. The decay energy has been measured by means of a coincidence technique. Six excited levels have been established for ^{185}Re, of which five had been postulated by earlier workers.

REFERENCES

Alaga, G., Alder, K., Bohr, A. and Mottelson, B.R. (1955). K. Danske Vidensk. Selsk., mat.-fys. Medd. 29, No. 9.

Band, I. M., Zyryanova, L.N. and Suslov, Y.P. (1958). Izv. Akad Nauk. SSSR Ser. fiz. 22, 952.

Bès, D.R. and Yi-chung, Cho. (1965). Nucl. Phys. 86, 581.

Bisgård, K.M., Nielsen, L.J., Stabell, E. and Ostergård, P. (1965). Nucl. Phys. 71, 192.

Bisgård, K.M. and Veje, E. (1967). Nucl. Phys. A103, 545.

Bohr, A. and Mottelson, B.R. (1953). K. Danske Vidensk. Selsk. mat.-fys. Medd. 27, No. 16.

de Boer, J., Martin, M. and Marmier, P. (1959). Helv. Phys. Acta 32, 377.

Brysk, H. and Rose, M.E. (1958). Rev. Mod. Phys. 30, 1169.

Bunker, M., Canada, R., and Mitchell, A.C.G. (1950). Phys. Rev. 79, 610.

Church, E.L. and Weneser, J. (1956). Phys. Rev. 104, 1382.

Cork, J.M., LeBlanc, J.M., Nester, W.H., Martin, D.W., and Brice, M.K. (1953). Phys. Rev. 90, 444.

Dzhelepov, B.S., Zhukovskiĭ, N.N. and Maloyan, A.G. (1966). J. Nucl. Phys. (U.S.S.R.) 3, 785.

Faessler, A. (1964). Nucl. Phys. 59, 177.

Feather, N. (1955). "Beta and Gamma Ray Spectroscopy" (Ed. K. Siegbahn), North Holland Publishing Co., Amsterdam.

Fermi, E. (1934). Zeits. f. Phys. 88, 1961.

Gallagher, C.J., Stromger, D. and Unik, J.P. (1958). Phys. Rev. 110, 725.

Gallagher, C.J., Edwards, W.F. and Manning, G. (1960). Nucl. Phys. 19, 18.

Geiger, J.S., Graham, R.L. and Ewan, G.T. (1960). Nucl.Phys. 16,1.

Gerholm, T.R. and Pettersson, B.G. (1963). "Role of Atomic Electrons in Nuclear Transformations", Proceedings of International Conference (Poland), Vol. I.

Gizon, J. and Boutet, J. (1967). Nucl. Phys. A103, 9.

Gizon, J. (1968). Nucl. Phys. A108, 425.

Goodman, L.J. and Pool, M.L. (1947). Phys. Rev. 71, 288.

Graham, R. L., Ewan, G.T. and Geiger, J.S. (1960). Nuclear Instruments and Methods 9, 245.

Hager, R.S. and Seltzer, E.C. (1968). Internal Conversion Tables. Part I: Nuclear Data A4, 1.

Haxel, O., Jensen, J.H.D. and Suess, H.E. (1949). Phys. Rev. 75, 1766.

Haxel, O., Jensen, J.H.D. and Suess, H.E. (1950). Z. Physik. 128, 295.

Heath, R.L. (1964). AEC Report IDO-16880-1.

Johns, M.W., Nablo, S.V. and King, W.J. (1957). Can. J. Phys. 35, 1159.

Katzin, L.I. and Poberskin, M. (1948). Phys. Rev. 96, 1599.

Lindgren, I. (1965). Tables in "Alpha-, Beta- and Gamma-Ray Spectroscopy" (Ed. K. Siegbahn), North Holland Publishing Co., Amsterdam.

McGowan, F.K. and Stelson, P.H. (1958). Phys. Rev. 109, 901.

Mayer, M.G. (1949). Phys. Rev. 75, 1969.

Mayer, M.G. (1950). Phys. Rev. 78, 16.

Metzger, F.R. (1967). Phys. Rev. 157, 1060.

Miller, M. and Wilkinson, R.G. (1951). Phys. Rev. 82, 981 L; 83, 1050L.

Mladjenović, M. and Slätis, H. (1955). Arkiv Fysik. 9, 41.

Mottelson, B.R. and Nilsson, S.G. (1959). Kgl. Danske Vidensk. Selsk. mat.-fys. Skr. 1, No. 8.

Newton, J.O. (1960). Phys. Rev. 117, 1529.

Nilsson, S.G. (1955). K. Danske Vidensk. Selsk. mat.-fys. Medd. 29, No. 16.

Pauli, W. (1934). Rapports du Septieme Conseil de Physique Solvay, Brussels, 1933, Paris: Gauthier-Villars et Cie.

Preston, M.A. (1962). "Physics of the Nucleus", Addison-Wesley Publishing Co. Inc., Reading, Mass., U.S.A.

Rao, P.V. and Crasemann, B. (1966). Phys. Rev. 142, 768.

Reines, F., Cowan, C.L., Harrison, F.B., McGuire, A.D. and Kruse, H.W. (1960). Phys. Rev. 117, 159.

Robinson, B.L. (1965). Nucl. Phys. 64, 1967.

Rose, M.E., Goertzel, G.H., Spinrad, B.I., Harr, J. and Strong, P. (1951). Phys. Rev. 83, 79.

Rose, M.B. (1958). "Internal Conversion Coefficients", North Holland Publishing Co., Amsterdam.

Schulz, G. (1967). Nucl. Phys. A101, 197.

Segrè, E. (1965). "Nuclei and Particles", W. A. Benjamin, Inc., New York.

Sliv, L.A. (1951). JETP 21, 790.

Sliv, L.A. and Band, I.M. (1956)."Coefficients of Internal Conversion of Gamma Radiation, Part I, K-Shell", Physico-Technical Institute, Academy of Science, Leningrad; (1958) Part II, L-shell.

Sliv, L.A. and Band, I.M. (1965). Tables in "Alpha-, Beta- and Gamma-Ray Spectroscopy" (Ed. K. Siegbahn). North Holland Publishing Co., Amsterdam.

Soloviev, V.G. and Vogel, P. (1966). Nucl. Phys. A92, 467.

Sujkowski, Z. (1961). Arkiv Fysik 20, 243.

Sunyar, A.W. (1955). Phys. Rev. 98, 653.

Swan, J.B. and Hill, R.D. (1952). Phys. Rev. 88, 831.

Wapstra, A.H. and Nijgh, G.J. (1956). Nucl. Phys. 1, 145.

Weisskopf , V.F. (1951). Phys. Rev. 83, 1073.

Zyryanova, L.N. (1963). "Once-Forbidden Beta-Transitions". The MacMillan Co., New York.